CrossMark

A SPECTROSCOPIC SURVEY OF THE FIELDS OF 28 STRONG GRAVITATIONAL LENSES: THE GROUP CATALOG

MICHELLE L. WILSON[1], ANN I. ZABLUDOFF[1], S. MARK AMMONS[2], IVELINA G. MOMCHEVA[3], KURTIS A. WILLIAMS[4], AND CHARLES R. KEETON[5]

[1] Steward Observatory, University of Arizona, 933 North Cherry Avenue, Tucson, AZ 85721, USA
[2] Lawrence Livermore National Laboratory, Physics Division L-210, 7000 East Avenue, Livermore, CA 94550, USA
[3] Space Telescope Science Institute, 3700 San Martin Drive, Baltimore, MD 21218, USA
[4] Department of Physics and Astronomy, Texas A&M University-Commerce, Commerce, TX, 75428, USA
[5] Department of Physics and Astronomy, Rutgers University, 136 Frelinghuysen Road, Piscataway, NJ 08854, USA
Received 2016 February 26; revised 2016 August 24; accepted 2016 September 10; published 2016 December 16

ABSTRACT

With a large, unique spectroscopic survey in the fields of 28 galaxy-scale strong gravitational lenses, we identify groups of galaxies in the 26 adequately sampled fields. Using a group-finding algorithm, we find 210 groups with at least 5 member galaxies; the median number of members is 8. Our sample spans redshifts of $0.04 \leqslant z_{\mathrm{grp}} \leqslant 0.76$ with a median of 0.31, including 174 groups with $0.1 < z_{\mathrm{grp}} < 0.6$. The groups have radial velocity dispersions of $60 \leqslant \sigma_{\mathrm{grp}} \leqslant 1200 \, \mathrm{km \, s^{-1}}$ with a median of $350 \, \mathrm{km \, s^{-1}}$. We also discover a supergroup in field B0712+472 at $z = 0.29$ that consists of three main groups. We recover groups similar to ~85% of those previously reported in these fields within our redshift range of sensitivity and find 187 new groups with at least five members. The properties of our group catalog, specifically, (1) the distribution of σ_{grp}, (2) the fraction of all sample galaxies that are group members, and (3) the fraction of groups with significant substructure, are consistent with those for other catalogs. The distribution of group virial masses agrees well with theoretical expectations. Of the lens galaxies, 12 of 26 (46%) (B1422+231, B1600 +434, B2114+022, FBQS J0951+2635, HE0435-1223, HST J14113+5211, MG0751+2716, MGJ1654+1346, PG 1115+080, Q ER 0047-2808, RXJ1131-1231, and WFI J2033-4723) are members of groups with at least five galaxies, and one more (B0712+472) belongs to an additional, visually identified group candidate. There are groups not associated with the lens that still are likely to affect the lens model; in six of 25 (24%) fields (excluding the supergroup), there is at least one massive ($\sigma_{\mathrm{grp}} \geqslant 500 \, \mathrm{km \, s^{-1}}$) group or group candidate projected within $2'$ of the lens.

Key words: catalogs – galaxies: groups: general – gravitational lensing: strong

Supporting material: figure set, machine-readable tables

1. INTRODUCTION

Gravitational lensing is an attractive method to measure cosmological parameters (e.g., Refsdal 1964; Oguri 2007; Suyu et al. 2013), because the lensing phenomenon only depends on the geometry of the universe and the mass distribution along the line of sight. However, determining this mass can be difficult. Many of the properties of lens systems (e.g., shears or lensed image positions) are not well described by a model with only one galaxy contributing to the lensing potential, showing that groups or clusters of galaxies at the lens and even along the line of sight of the lens are important to the lensing (e.g., Keeton et al. 1997; Lehar et al. 1997; Keeton & Zabludoff 2004; Wambsganss et al. 2005; Jaroszynski & Kostrzewa-Rutkowska 2012; Collett et al. 2013).

Galaxy groups are interesting in addition to their possible impact on gravitational lensing because they are important to galaxy evolution. Groups are the most common environment for galaxies, with even our own Milky Way residing in the Local Group. Their lower velocity dispersions foster stronger galaxy–galaxy interactions than do clusters (e.g., Zabludoff & Mulchaey 1998). Moreover, cluster galaxy properties, such as mass or color, may first develop through "pre-processing" in the less dense group environment (e.g., Zabludoff et al. 1996; Zabludoff & Mulchaey 1998; McGee et al. 2009; Just et al. 2015).

To produce a new group sample with which to investigate the environments of lens systems and line-of-sight structures as well as the effect of environment on galaxy properties, we employ a spectroscopic survey in the fields of 28 galaxy-scale strong

gravitational lenses (Momcheva et al. 2015). In 26 of these fields, we construct a group-finding algorithm that works well for spectroscopic samples of variable completeness, field size, and sampling footprint, modifying the iterative method of Ammons et al. (2014). Our method is also designed to find a range of group masses without favoring the most dynamically evolved systems (i.e., those with a significant quiescent galaxy population and/or detectable hot intracluster gas), unlike methods that use galaxy color, galaxy luminosity, or X-ray halo detections to identify groups or determine group properties. The resulting catalog includes groups ranging from very poor ($\sigma_{\mathrm{grp}} \sim 100 \, \mathrm{km \, s^{-1}}$) to rich clusters (~1000 $\mathrm{km \, s^{-1}}$) at $0.04 \leqslant z \leqslant 0.76$.

In this paper, we describe the data (Section 2), our group finding algorithm (Section 3), and its performance (Section 4). We present our group catalog and discuss its properties in Section 5.1, describe a supergroup we identify in Section 5.2, and comment on the lens environments and line-of-sight structures in Sections 5.3 and 5.4, respectively. We suggest ways of using our catalog and group quality flags for various science cases in Section 6.

Throughout this paper, we adopt the values of $H_0 = 71 \, \mathrm{km \, s^{-1} \, Mpc^{-1}}$, $\Omega_m = 0.274$, and $\Omega_{\Lambda} = 0.726$ (Hinshaw et al. 2009).

2. THE DATA

2.1. Photometry

Images of each lens field were collected using the Mosaic-1 imager on the Kitt Peak National Observatory Mayall 4 m

telescope and the Mosaic-2 imager on the Cerro Tololo Inter-American Observatory Blanco 4 m telescope. Williams et al. (2006) detail these data and their reduction, which we summarize here. Each field was imaged using the "nearly Mould" I-band filter, as well as either the Harris V filter or the Harris R filter, depending on the redshift at which the 4000 Å break of the lens galaxy enters the R filter ($z \geqslant 0.35$). Photometry was obtained using the routine MAG_AUTO of the SExtractor version 2.3.2 (Bertin & Arnouts 1996). Galaxy colors were measured using aperture magnitudes after degrading one image to match the seeing of the other. The photometry was then calibrated to the Kron–Cousins filter set using the imaging of the Landolt (1992) standard star fields. The photometry was used to select objects for spectroscopic follow-up and to calculate spectroscopic completeness.

2.2. Spectroscopy

The spectroscopic follow-up is described in Momcheva et al. (2015). We summarize the most pertinent details here.

A sample of objects from the photometry was selected for spectroscopic follow-up using Hectospec on the MMT 6.5 m telescope and LDSS-2, LDSS-3, and IMACS on the Magellan 6.5 m telescopes.

Priorities were ranked in the following manner. Objects identified as potential members of a red sequence (Williams et al. 2006), regardless of whether that sequence is at the lens redshift, were given the highest priority. Objects outside potential red sequences, but redder than models of starburst galaxies at the lowest redshift candidate red sequence, bluer than members of the highest redshift candidate red sequence, and within $5'$ of the lens in each field were given second highest priority. Objects outside this color range, but within $5'$ of the lens were given third highest priority. Finally, objects farther than $5'$ from the lens were given the lowest priority. The limiting magnitude for spectroscopic targeting was either 20.5 or 21.5, depending on the instrument used.

This target selection method results in a strong radial gradient in the spectroscopic completeness. Some fields have patchy completeness because of the multislit mask designs. Furthermore, the spectroscopic completeness varies greatly from field to field; within $2'$ of the lens, completenesses range from ~20% to 90% (see Figures 5, 36, and 37 in Momcheva et al. 2015). Hectospec uses fibers with large holders that cannot be placed more closely on the sky than $20''$, and the northern fields typically have fewer configurations. Thus, fields observed with this instrument have sparser but smoothly varying radial completeness over our full field of view. Those observed with LDSS-2, LDSS−3, and IMACS in many cases display a rectangular and/or patchy completeness that is inconsistent with the total available aperture of the instrument (see Figure Set 7, e.g., fields b1422 and q1017). These distributions were due to the mask designs. Early LDSS-2 masks were all centered on the lens, resulting in higher completeness within $5'$ from the lens. Later observations were planned assuming a five-mask configuration tiled in the shape of the pips on the "five side" of a die, with one mask in the middle and four masks that slightly overlapped each other arranged in a square. The sampled field of view generally extends to at least $1r_{\rm vir}$ for groups with velocity dispersions of up to ~500 km s^{-1} at $z \gtrsim 0.1$ and for richer clusters with velocity dispersions of up to ~900 km s^{-1} at $z \gtrsim 0.2$.

Four fields (he0435, q0047, q0158, and rxj1131) were imaged while one of the eight CCDs in the Mosaic-2 camera was non-operational in late 2003. This resulted in a dearth of imaging data over a ~$9' \times 18'$ region in the eastern portion of each field. Since the spectroscopic targets were selected from our photometry, these regions have no spectroscopic coverage.

For 2 of the 28 fields, b1608 and pmn2004, the spectroscopic completenesses are very low because of the limited spectroscopic observations. Thus, we do not include these fields in our group catalog.

Redshifts were calculated with a routine based on that of Cool et al. (2008), which involves a χ^2 fit of the measured spectra to templates. The resulting redshifts of objects observed with IMACS and LDSS-3 were checked visually against the sky-subtracted, two-dimensional spectra. The median uncertainty on the redshifts is ~0.0002, or ~60 km s^{-1} at $z = 0.3$.

Additional objects with published redshifts taken from NED[6] were included as well. In two fields, the NED additions were significant. There were 240 NED additions to h12531, as it includes a previously studied supercluster at $z = 1.237$ (Demarco et al. 2007), and 133 to pg1115, which includes the $z = 0.485$ cluster RXJ1117.4+0743. These additions are visible in the sky plots as small densely sampled regions near the edges of our fields.

We note that our algorithm (see Section 3.1 and Appendix A) is not optimized for the relatively overdense patches arising from adding many NED redshifts in the fields h12531 and pg1115. Before running the group algorithm, we therefore discarded the galaxies obtained from NED in these two fields that have I-band magnitudes fainter than 21.5 mag (165 galaxies in field 12531 and 21 galaxies in field pg1115) to make the magnitude limits of those fields better comparable to the rest of our survey. In h12531, this cut removes many galaxies at $z \sim 1.24$. Since our work is optimized at $z < 1$, we refer to Demarco et al. (2007) and Tanaka et al. (2009) for further details.

In field sbs1520, the lens galaxy has two contradictory redshifts available in the literature: $z = 0.72$ from Chavushyan et al. (1997) and $z = 0.761$ from Auger et al. (2008). Thus, neither one appears in our redshift catalog, although both are marked in plots when relevant.

The final redshift catalog includes 9662 unique galaxies. This catalog includes 9370 galaxies that are not in the preliminary catalog and analysis presented in Momcheva et al. (2006), most of which are in 20 additional fields.

To determine the redshift interval over which each field is most sensitive, we consider the spectroscopic field size and how the spectroscopic completeness varies over our I-band magnitude range. We assume a homogeneous universe, use the luminosity functions of Faber et al. (2007) for $0 < z < 1$, and implement K-corrections using an LRG spectral template, as in Ammons et al. (2014). Although the selection functions vary slightly from field to field, the peak is at $z \sim 0.2$–0.25, with generally high sensitivity from $0.05 < z < 0.5$. The survey sensitivity decreases at $z \gtrsim 0.5$; so, it is more difficult for us to identify structures at these higher redshifts.

3. FINDING GROUPS

Several group and cluster identification methods exist in the literature. Massive dynamically evolved low-redshift structures can be readily detected in X-ray observations (e.g., Lloyd-Davies et al. 2011), as can clusters at all redshifts via the Sunyaev–Zeldovich effect (e.g., Bleem et al. 2015; Planck Collaboration et al. 2015). However, these methods also require some member galaxy redshifts to determine the structure's redshift.

Other group finders rely on additional sources of data, such as photometry and/or photometric redshifts, to locate groups using adaptive matched filters (e.g., Szabo et al. 2011), red-sequence identification (e.g., Williams et al. 2006; Koester et al. 2007), or low surface brightness enhancement identification (e.g., Gonzalez et al. 2001; White et al. 2005). These methods can be useful, especially when the spectroscopic data are sparse compared with the amount of photometric information available, but are typically more sensitive to massive evolved systems.

Since even low-mass groups can affect gravitational lensing models, we require a method that is sensitive to less massive systems as well as clusters. One such approach is to compile large spectroscopic samples and then search for spatial and redshift clustering. The friends-of-friends (Huchra & Geller 1982) and the Voronoi-Delaunay (Marinoni et al. 2002) methods are commonly used. These techniques can be useful for uniformly complete redshift samples, but cannot be used for samples with large spatial variations in spectroscopic completeness, which we have; in this situation, iterative methods, such as that of Wilman et al. (2005), are more appropriate.

3.1. Algorithm

We use the iterative approach of Ammons et al. (2014) after modification to accommodate our spectroscopic sample and to find less massive structures. We develop a two-phase process where we identify candidate density peaks based on galaxy overdensities in velocity and spatial projection and then iterate for the galaxy membership and group properties. The main differences between our method and that of Ammons et al. (2014) are the method of generating candidate density peaks, the projected spatial criteria in the membership iteration, and the parameter values we choose. We automate the peak-finding process. We do not use any magnitude or color information to identify candidate groups, because we wish to be able to find lower mass groups without prominent red sequences as well as rich clusters. The resulting group catalog is produced algorithmically, with parameter choices justified in this section and in Appendix A; only one system, a complex supergroup, is altered after the fact (see Section 5.2). Our algorithm is tuned to select groups that we visually identify, but applies criteria uniformly so that our resulting group catalog is reproducible. It also finds some groups with similar properties that were not visually identified.

There are nine parameters in our method of selecting candidate peaks and determining group membership, some of which are degenerate, leading to multiple ways to achieve roughly the same ends. We require our catalog to include most of the likely structures we identify by eye as obvious overdensities of galaxies in velocity and projected spatial position (see Section 3.2). We also aim to minimize the number of structures with unphysically large velocity dispersions. Although there is some variation in the exact group catalog, most of the groups are stable to small changes in the parameters. We test the "realness" of our groups in Section 4.

The steps of our algorithm are as follows:

1. We identify overdensities of galaxies in velocity by binning the galaxies in $1200 \, \mathrm{km \, s^{-1}}$ wide bins (three times the velocity dispersion of that of typical groups we expect). This method relies on the uncertainties in redshift, and consequently velocity, being small compared to the velocity bin width, as is the case for our sample, so that galaxies can be robustly binned. We use the same bin width for all redshifts, although this velocity interval will correspond to a varying rest frame velocity dispersion. We select velocity bins with at least five galaxies. We then shift the velocity bins five times by steps of $200 \, \mathrm{km \, s^{-1}}$, half the expected velocity dispersion for a typical group in our sample, and again select the velocity bins with at least five galaxies. These multiple velocity bin positions reduce the chance of a group being missed because its members were split by a velocity bin boundary and increases the chance for groups to be well centered in a velocity bin. We do not use a spatial selection in this step, but do so in the next step below.

2. We look for spatial overdensities of the galaxies within these velocity bins.

   We divide the observed field into grid squares $3.3 r_{\mathrm{vir}}$ on a side, assuming a group-like velocity dispersion of $400 \, \mathrm{km \, s^{-1}}$ and using the formula for r_{200} given by Carlberg et al. (1997) as an approximation of the virial radius:

   $$r_{\mathrm{vir},\sigma} \approx r_{200} = \frac{\sqrt{3} \, \sigma_{\mathrm{grp}}}{10 H(z)}, \qquad (1)$$

   where

   $$H(z) = H_0 \sqrt{\Omega_m (1 + z_{\mathrm{gal}})^3 + \Omega_\Lambda} \qquad (2)$$

   for a flat cosmology, and z_{gal} corresponds to the lower boundary of the velocity bin. We center the grid on the median R.A. and decl. of the galaxies in each bin. We do not treat the lens galaxy as special in this or in any other step of the group finder. We define each grid square with five or more galaxies as a "candidate peak" and calculate its median redshift, R.A., and decl. We use these quantities as starting points for our iterative group member identification. We repeat this candidate peak finder nine more times, centering the grid in different positions (shifting it a quarter of a grid square in R.A., a quarter of a grid square in decl., and a quarter of a grid square in both R.A. and decl.). These multiple positions increase the likelihood of identifying multiple overdensities of galaxies in a single velocity bin as candidate peaks if one (or more) is split by a grid square boundary for one grid position and increases the likelihood of groups being well-centered in at least one grid position. We use all the candidate peaks generated in all of these grid positions for all of these velocity bin phases, even though some are different parts of the same structures. The combination of velocity bin width, grid square size, velocity dispersion, and number of galaxies per bin or grid square is chosen so the resulting group catalog best reproduces our initial visual identifications discussed in the next section.

3. We optimize the group membership using these candidate peaks as starting points. We select galaxies within a redshift interval Δz of the candidate peak redshift and $3 r_{\mathrm{vir}}$ from the

peak's projected spatial centroid assuming a velocity dispersion of $400 \, \mathrm{km \, s^{-1}}$. We choose a Δz that corresponds to $6600 \, \mathrm{km \, s^{-1}}$ at the candidate peak's redshift, which corresponds to $\pm$ three times the velocity dispersion of a Coma-sized cluster. We select a large Δz compared with our initially assumed velocity dispersion to avoid excluding galaxies in the high-velocity tails should the identified peak correspond to a higher velocity dispersion structure, as would become evident during the membership optimization process described below. Using these galaxies, we calculate the biweight redshift (z_{grp}), mean position, and the cosmologically corrected biweight line-of-sight velocity dispersion (σ_{grp}). We then select the galaxies within $3\sigma_{\mathrm{grp}}$ of this new mean redshift after transforming the velocity dispersion to a redshift interval using

$$\Delta z = \frac{3\sigma_{\mathrm{grp}}}{c}, \tag{3}$$

and within $3r_{\mathrm{vir}}$, using z_{grp}, of the spatial centroid.

In the first iteration, we also reject members that are more than a velocity dispersion away from their nearest neighbor in velocity, as they are unlikely to be members. This choice has an effect on roughly 20% of the catalog, generally one or more galaxies being removed in the outskirts of the group as projected on the sky; the new group redshift and/or velocity dispersion differs by more than three times the error in z_{grp} or σ_{grp}, respectively, for ~1% of the groups. There are an additional 19 groups with at least 5 members when clipping is not performed, but a structure with an unlikely large velocity dispersion is also identified. Thus, we choose to perform this clipping to reduce the identification of galaxies as group members that are in the tails of both the group velocity and spatial distributions and minimize unrealistically large structures.

Using the galaxies that satisfy these cuts in velocity and position, we recalculate the mean redshift and spatial centroid and find the resulting membership. We recalculate the group parameters and redetermine the galaxies within $3\sigma_{\mathrm{grp}}$ of the mean redshift and $3r_{\mathrm{vir}}$ of the spatial centroid for 10 total iterations. We consider a group to have converged if the membership does not change in the last 3 iterations. Given our field boundaries, groups at low redshift and/or with large velocity dispersions may be sampled to less than $3r_{\mathrm{vir}}$. We flag any group not sampled to at least $1r_{\mathrm{vir}}$ in the catalog tables (Tables 1, 2, and 4).

4. Large structures may have member galaxies spread over a projected area larger than $3r_{\mathrm{vir}}$ when a velocity dispersion of $400 \, \mathrm{km \, s^{-1}}$ is assumed, therefore our binning and gridding systems might generate multiple candidate peaks for a single structure. Because our iterative procedure can find the true larger group, these multiple candidate peaks may converge on identical or overlapping groups. Thus, we must remove duplicate groups and combine nearly identical groups (see Appendix A for details). If multiple candidate peaks converge on multiple identical group memberships, we select one of the identical groups without rerunning the algorithm. If in more than 75% of the trials a group converges with the same membership, we add that group to our catalog. In other cases, where a group shares at least 50% of its members with another, we determine the mean of these groups' spatial centroids, redshifts, velocity dispersions, and virial radii, and reiterate on the

membership to produce a single group for the catalog. If between 0% and 50% of a group's members are also assigned to another group, we determine to which group the galaxies are more likely to be bound and remove them from the other (see Appendix A.3).

For these groups, we calculate virial masses. There are two ways to determine the masses of structures: via the projected harmonic mean radius (R_{PV}), and solely via the velocity dispersion. Biviano et al. (2006) find that the $M_{\mathrm{vir}, R_{\mathrm{PV}}}$ and $r_{\mathrm{vir}, R_{\mathrm{PV}}}$ are overestimated for small sample sizes, whereas $M_{\mathrm{vir}, \sigma}$ and $r_{\mathrm{vir}, \sigma}$ are not biased.

As for the virial radius, to approximate the virial mass, we use the formula for M_{200} derived by Munari et al. (2013) from simulations, fit over the mass range of $10^{13} \lesssim M_{200} \lesssim 10^{15} \, M_{\odot}$,

$$M_{\mathrm{vir}, \sigma} \approx M_{200} = \frac{10^{15} \, M_{\odot}}{h(z)} \left(\frac{\sigma_{\mathrm{grp}}}{A_{\mathrm{1D}}} \right)^{(1/\alpha)}, \tag{4}$$

where $h(z) = H(z)/(100 \, \mathrm{km \, s^{-1} \, Mpc^{-1}})$. We take $A_{\mathrm{1D}} = 1177 \, \mathrm{km \, s^{-1}}$ and $\alpha = 0.364$ from their simulations using AGN feedback and galaxy tracers. Compared to these, R_{PV}-based virial masses ($M_{\mathrm{vir}, R_{\mathrm{PV}}}$) using the equations of Girardi et al. (1998) and Limber & Mathews (1960) are systematically higher by ~0.6 dex over most of the mass range of our final catalog. This offset creates a high-mass tail that consists of 14 groups with $M_{\mathrm{vir}} > 10^{15} \, M_{\odot}$ for $0.2 < z_{\mathrm{grp}} < 0.5$ that is not in agreement with the high-mass slope of the Millennium-XXL (MXXL) cosmological simulation (Angulo et al. 2012) given any arbitrary volume normalization (see Section 4.2.3). Furthermore, $r_{\mathrm{vir}, R_{\mathrm{PV}}}$ is about 1.5 times larger than both $r_{\mathrm{vir}, \sigma}$ and that expected for NFW halos.

Thus, our data support the conclusions of Biviano et al. (2006) and motivate our use of $r_{\mathrm{vir}, \sigma}$ and $M_{\mathrm{vir}, \sigma}$. These choices differ from those made in Ammons et al. (2014), who calculate R_{PV} and $M_{\mathrm{vir}, R_{\mathrm{PV}}}$.

We only report masses $\geqslant 10^{13} \, M_{\odot}$. The M_{vir} relation we adopt has not been calibrated for lower masses. Lower masses (i.e., those in the range normally expected for single massive galaxy halos rather than virialized groups) are likely to be underestimated because of the incomplete group member identification.

All uncertainties in group quantities are calculated using a bootstrap method with 1000 iterations. We resample with replacement of the identified group members and recalculate the group properties using the resampled members. We then subtract the median value of each property over all the iterations and find the 16th and 84th percentile values, which are listed in the tables with the properties measured using all the algorithmically identified group members.

Our group catalog and individual group memberships are likely to be somewhat incomplete, although we show below that our catalog reproduces the distributions of group kinematic properties and the fraction of group members to field galaxies of other catalogs in the literature (Section 4.2). Here we perform a simple test of how incompleteness might affect the derived group centroids, velocity dispersions, and masses. For the 32 groups with at least 20 members, we randomly select 25%, 50%, and 75% of their members without replacement 1000 times and find the median group parameter values. For all three incompleteness levels, the median values are within three

Table 1
Algorithmically Identified Groups With $\geqslant 5$ Members

Field	Group	N_m	$z_{\rm grp}$	$\overline{\rm R.A.}$ (deg)	$\overline{\rm Decl.}$ (deg)	$R^{\rm b}$ (′)	$\sigma_{\rm grp}$ (km s^{-1})	$M_{\rm vir}^{\rm c}$ ($10^{13}\,M_\odot$)	$r_{\rm vir}$ (Mpc)	Flag[d]	Match[e]
b0712	0	5	$0.0784^{+0.0002}_{-0.0003}$	$109.0365^{+0.0541}_{-0.0524}$	$46.8814^{+0.0112}_{-0.0112}$	15.99	140^{+30}_{-110}	⋯	0.34	1, 3	⋯
	3	34	$0.3723^{+0.0007}_{-0.0007}$	$109.1105^{+0.0226}_{-0.0225}$	$47.0370^{+0.0263}_{-0.0226}$	7.68	870^{+70}_{-70}	$51.5^{+12.5}_{-10.6}$	1.78	4	⋯
	5	6	$0.4146^{+0.0003}_{-0.0003}$	$108.6920^{+0.0097}_{-0.0102}$	$47.0648^{+0.0126}_{-0.0108}$	14.10	180^{+40}_{-60}	⋯	0.35	⋯	⋯
	7	5	$0.4938^{+0.0007}_{-0.0006}$	$109.0083^{+0.0171}_{-0.0172}$	$47.0681^{+0.0086}_{-0.0086}$	4.77	270^{+50}_{-230}	$2.0^{+0.9}_{-1.3}$	0.52	⋯	⋯
b1152	0	10	$0.0514^{+0.0006}_{-0.0003}$	$178.8423^{+0.0505}_{-0.0486}$	$19.7020^{+0.0247}_{-0.0269}$	2.58	480^{+90}_{-350}	$11.9^{+6.2}_{-9.9}$	1.15	1, 2	⋯
	1	5	$0.1314^{+0.0002}_{-0.0002}$	$178.8226^{+0.0079}_{-0.0079}$	$19.7307^{+0.0145}_{-0.0145}$	4.14	130^{+40}_{-100}	⋯	0.31	⋯	⋯
	2	5	$0.1579^{+0.0002}_{-0.0003}$	$178.7729^{+0.0250}_{-0.0249}$	$19.4936^{+0.0140}_{-0.0140}$	10.53	190^{+50}_{-50}	⋯	0.44	⋯	⋯
	3	6	$0.1624^{+0.0000}_{-0.0003}$	$178.7169^{+0.0050}_{-0.0050}$	$19.4548^{+0.0132}_{-0.0135}$	13.88	90^{+30}_{-70}	⋯	0.21	⋯	⋯
	4	21	$0.1706^{+0.0005}_{-0.0005}$	$178.9860^{+0.0314}_{-0.0295}$	$19.6834^{+0.0318}_{-0.0302}$	9.11	530^{+50}_{-80}	$14.4^{+3.8}_{-4.8}$	1.19	⋯	⋯
	5	8	$0.1982^{+0.0003}_{-0.0004}$	$179.0379^{+0.0147}_{-0.0165}$	$19.8251^{+0.0136}_{-0.0128}$	15.45	210^{+30}_{-120}	$1.1^{+0.5}_{-0.8}$	0.47	⋯	⋯
	6	12	$0.2394^{+0.0006}_{-0.0006}$	$178.7031^{+0.0165}_{-0.0204}$	$19.7545^{+0.0181}_{-0.0186}$	8.92	420^{+140}_{-130}	$7.4^{+7.0}_{-3.6}$	0.91	4	⋯
	7	7	$0.2396^{+0.0003}_{-0.0007}$	$178.9859^{+0.0259}_{-0.0211}$	$19.7547^{+0.0111}_{-0.0107}$	10.59	380^{+260}_{-130}	$5.6^{+6.4}_{-0.5}$	0.83	⋯	⋯
	8	60	$0.3272^{+0.0006}_{-0.0006}$	$178.8247^{+0.0174}_{-0.0159}$	$19.7320^{+0.0151}_{-0.0153}$	4.22	1010^{+60}_{-70}	$78.8^{+12.8}_{-13.2}$	2.11	⋯	⋯
	9	7	$0.3660^{+0.0019}_{-0.0008}$	$178.9210^{+0.0098}_{-0.0082}$	$19.7865^{+0.0088}_{-0.0082}$	9.20	480^{+410}_{-30}	$10.2^{+8.8}_{-0.02}$	0.99	⋯	⋯
	10	25	$0.3788^{+0.0008}_{-0.0007}$	$178.9192^{+0.0164}_{-0.0152}$	$19.6569^{+0.0181}_{-0.0164}$	5.25	650^{+50}_{-70}	$23.4^{+5.5}_{-5.8}$	1.33	⋯	⋯
	11	5	$0.3899^{+0.0008}_{-0.0004}$	$178.7916^{+0.0093}_{-0.0093}$	$19.7350^{+0.0116}_{-0.0116}$	4.82	270^{+50}_{-180}	$2.0^{+0.9}_{-1.2}$	0.54	⋯	⋯
	12	35	$0.4514^{+0.0006}_{-0.0006}$	$178.9092^{+0.0101}_{-0.0105}$	$19.5389^{+0.0102}_{-0.0093}$	8.73	600^{+50}_{-70}	$18.1^{+4.6}_{-4.9}$	1.18	⋯	⋯
b1422	0	9	$0.0724^{+0.0005}_{-0.0005}$	$216.2106^{+0.0319}_{-0.0261}$	$22.9808^{+0.0482}_{-0.0465}$	4.03	480^{+120}_{-310}	$11.6^{+8.3}_{-8.8}$	1.13	1, 2	⋯
	1	12	$0.1453^{+0.0007}_{-0.0005}$	$216.1938^{+0.0288}_{-0.0274}$	$22.9031^{+0.0361}_{-0.0338}$	2.66	380^{+50}_{-60}	$6.1^{+2.4}_{-2.1}$	0.88	⋯	⋯
	2	17	$0.2829^{+0.0007}_{-0.0005}$	$216.1578^{+0.0131}_{-0.0137}$	$22.9535^{+0.0185}_{-0.0174}$	1.20	430^{+50}_{-70}	$7.5^{+2.6}_{-2.7}$	0.91	⋯	⋯
	4[a]	23	$0.3385^{+0.0005}_{-0.0005}$	$216.1829^{+0.0090}_{-0.0082}$	$22.9341^{+0.0115}_{-0.0120}$	1.34	460^{+60}_{-50}	$9.0^{+3.3}_{-2.4}$	0.95	⋯	WMKZL06
	5	6	$0.3484^{+0.0005}_{-0.0004}$	$216.1629^{+0.0136}_{-0.0126}$	$22.9466^{+0.0107}_{-0.0096}$	0.82	270^{+50}_{-130}	$2.1^{+1.0}_{-1.4}$	0.56	⋯	⋯
	6	13	$0.3627^{+0.0008}_{-0.0009}$	$216.1306^{+0.0165}_{-0.0179}$	$22.9223^{+0.0207}_{-0.0194}$	1.69	690^{+90}_{-130}	$26.9^{+10.5}_{-10.5}$	1.41	⋯	⋯
b1600	0	5	$0.0600^{+0.0002}_{-0.0001}$	$240.3491^{+0.0341}_{-0.0287}$	$43.0618^{+0.0127}_{-0.0127}$	13.43	80^{+80}_{-10}	⋯	0.18	1, 3	⋯
	1	5	$0.0720^{+0.0001}_{-0.0000}$	$240.3218^{+0.0294}_{-0.0294}$	$43.1878^{+0.0055}_{-0.0055}$	6.96	90^{+20}_{-70}	⋯	0.21	1	⋯
	2	13	$0.1312^{+0.0003}_{-0.0005}$	$240.6064^{+0.0504}_{-0.0530}$	$43.2426^{+0.0258}_{-0.0252}$	8.50	370^{+130}_{-120}	$5.5^{+5.2}_{-2.4}$	0.85	3	⋯
	3	10	$0.2390^{+0.0009}_{-0.0010}$	$240.4225^{+0.0503}_{-0.0519}$	$43.3202^{+0.0172}_{-0.0155}$	2.43	540^{+100}_{-340}	$14.6^{+7.4}_{-10.2}$	1.17	⋯	⋯
	4	10	$0.2484^{+0.0006}_{-0.0007}$	$240.6052^{+0.0396}_{-0.0376}$	$43.1157^{+0.0166}_{-0.0140}$	12.79	470^{+100}_{-120}	$10.0^{+6.0}_{-4.9}$	1.02	3	⋯
	7	24	$0.2893^{+0.0005}_{-0.0005}$	$240.4396^{+0.0174}_{-0.0187}$	$43.2660^{+0.0222}_{-0.0193}$	1.23	510^{+50}_{-60}	$12.4^{+3.7}_{-3.3}$	1.09	⋯	AFALS07
	8[a]	6	$0.4146^{+0.0002}_{-0.0002}$	$240.4150^{+0.0032}_{-0.0039}$	$43.2758^{+0.0038}_{-0.0038}$	0.29	110^{+20}_{-20}	⋯	0.22	⋯	AFALS07
b2114	0	19	$0.0484^{+0.0003}_{-0.0003}$	$319.1814^{+0.0379}_{-0.0388}$	$2.5138^{+0.0359}_{-0.0377}$	5.36	360^{+60}_{-60}	$5.4^{+2.5}_{-2.0}$	0.87	1, 2	⋯
	2	17	$0.2025^{+0.0012}_{-0.0007}$	$319.2485^{+0.0293}_{-0.0322}$	$2.4502^{+0.0379}_{-0.0428}$	2.52	820^{+90}_{-90}	$47.6^{+14.6}_{-13.2}$	1.82	⋯	⋯
	3	34	$0.2251^{+0.0006}_{-0.0007}$	$319.3051^{+0.0186}_{-0.0179}$	$2.4065^{+0.0200}_{-0.0195}$	5.77	990^{+130}_{-150}	$78.1^{+28.8}_{-26.1}$	2.17	⋯	⋯
	5	19	$0.3068^{+0.0005}_{-0.0005}$	$319.1954^{+0.0106}_{-0.0096}$	$2.4002^{+0.0100}_{-0.0099}$	2.02	380^{+60}_{-80}	$5.4^{+2.3}_{-2.3}$	0.80	⋯	⋯
	7[a]	10	$0.3143^{+0.0002}_{-0.0002}$	$319.2143^{+0.0046}_{-0.0022}$	$2.4226^{+0.0048}_{-0.0048}$	0.45	140^{+30}_{-30}	⋯	0.30	⋯	WMKZL06
bri0952	0	8	$0.0929^{+0.0005}_{-0.0004}$	$148.7863^{+0.0564}_{-0.0539}$	$-1.4417^{+0.0431}_{-0.0410}$	4.19	270^{+40}_{-160}	$2.3^{+0.8}_{-1.5}$	0.62	1, 2	⋯
	1	10	$0.1376^{+0.0004}_{-0.0004}$	$148.6531^{+0.0296}_{-0.0273}$	$-1.4650^{+0.0394}_{-0.0354}$	6.24	350^{+90}_{-120}	$4.8^{+3.6}_{-2.6}$	0.81	3	⋯
	2	9	$0.1636^{+0.0004}_{-0.0004}$	$148.7295^{+0.0204}_{-0.0180}$	$-1.4736^{+0.0362}_{-0.0323}$	2.11	310^{+80}_{-100}	$3.5^{+2.5}_{-1.9}$	0.71	⋯	⋯
	4	12	$0.4201^{+0.0004}_{-0.0005}$	$148.7391^{+0.0072}_{-0.0076}$	$-1.4830^{+0.0114}_{-0.0099}$	1.31	330^{+60}_{-70}	$3.5^{+1.9}_{-1.5}$	0.66	⋯	⋯
	5	13	$0.4740^{+0.0007}_{-0.0007}$	$148.7654^{+0.0143}_{-0.0130}$	$-1.4918^{+0.0092}_{-0.0097}$	1.08	490^{+80}_{-100}	$9.8^{+4.9}_{-4.2}$	0.94	⋯	⋯
fbq0951	0	5	$0.0514^{+0.0001}_{-0.0002}$	$147.8052^{+0.0188}_{-0.0188}$	$26.5383^{+0.0244}_{-0.0244}$	3.61	80^{+50}_{-30}	⋯	0.18	1	⋯
	1	5	$0.0573^{+0.0004}_{-0.0002}$	$147.8515^{+0.0662}_{-0.0661}$	$26.6468^{+0.0444}_{-0.0423}$	3.60	190^{+40}_{-40}	⋯	0.45	1	⋯
	2	11	$0.0835^{+0.0015}_{-0.0008}$	$147.7701^{+0.0655}_{-0.0619}$	$26.5638^{+0.0487}_{-0.0468}$	4.22	500^{+120}_{-310}	$12.7^{+7.1}_{-6.7}$	1.17	1	⋯
	3	6	$0.1026^{+0.0001}_{-0.0001}$	$147.9898^{+0.0031}_{-0.0030}$	$26.5023^{+0.0150}_{-0.0148}$	9.33	80^{+20}_{-20}	⋯	0.19	⋯	⋯
	4	30	$0.1284^{+0.0016}_{-0.0016}$	$147.8553^{+0.0257}_{-0.0248}$	$26.5695^{+0.0234}_{-0.0212}$	1.22	1180^{+190}_{-370}	$134.8^{+61.6}_{-74.6}$	2.73	2	⋯
	5	8	$0.1571^{+0.0008}_{-0.0006}$	$147.8018^{+0.0500}_{-0.0421}$	$26.5714^{+0.0469}_{-0.0484}$	2.46	460^{+100}_{-320}	$9.7^{+5.3}_{-6.5}$	1.04	⋯	⋯
	6	26	$0.2105^{+0.0007}_{-0.0007}$	$147.7738^{+0.0283}_{-0.0242}$	$26.5915^{+0.0370}_{-0.0351}$	3.78	750^{+70}_{-80}	$37.5^{+10.4}_{-9.5}$	1.67	⋯	⋯
	7	7	$0.2379^{+0.0003}_{-0.0005}$	$147.9947^{+0.0199}_{-0.0185}$	$26.6590^{+0.0137}_{-0.0128}$	9.15	220^{+100}_{-90}	$1.2^{+1.6}_{-0.5}$	0.47	⋯	⋯
	8	6	$0.2511^{+0.0001}_{-0.0002}$	$147.8749^{+0.0049}_{-0.0049}$	$26.5903^{+0.0034}_{-0.0035}$	1.66	80^{+20}_{-50}	⋯	0.18	⋯	⋯
	9	11	$0.2515^{+0.0002}_{-0.0003}$	$147.7126^{+0.0112}_{-0.0148}$	$26.5066^{+0.0082}_{-0.0096}$	8.56	190^{+60}_{-80}	⋯	0.42	⋯	⋯
	10[a]	21	$0.2643^{+0.0008}_{-0.0007}$	$147.9281^{+0.0140}_{-0.0148}$	$26.6483^{+0.0207}_{-0.0257}$	5.80	660^{+100}_{-130}	$25.6^{+9.8}_{-9.0}$	1.43	⋯	⋯
	11	12	$0.3068^{+0.0006}_{-0.0005}$	$147.6851^{+0.0190}_{-0.0164}$	$26.6620^{+0.0113}_{-0.0113}$	9.64	410^{+60}_{-70}	$6.5^{+2.7}_{-2.3}$	0.86	⋯	⋯
	12	51	$0.3120^{+0.0002}_{-0.0003}$	$147.9765^{+0.0081}_{-0.0082}$	$26.5260^{+0.0084}_{-0.0074}$	8.00	450^{+50}_{-50}	$8.5^{+2.5}_{-2.2}$	0.94	4	⋯
	17	5	$0.3536^{+0.0006}_{-0.0002}$	$147.9895^{+0.0067}_{-0.0068}$	$26.5427^{+0.0176}_{-0.0176}$	8.25	250^{+70}_{-220}	$1.6^{+1.3}_{-1.2}$	0.51	⋯	⋯
	18	6	$0.3537^{+0.0004}_{-0.0004}$	$147.8054^{+0.0128}_{-0.0122}$	$26.5614^{+0.0140}_{-0.0135}$	2.59	220^{+50}_{-70}	$1.2^{+0.7}_{-0.6}$	0.45	⋯	⋯
	19	5	$0.3588^{+0.0003}_{-0.0008}$	$147.6718^{+0.0128}_{-0.0123}$	$26.3742^{+0.0093}_{-0.0088}$	15.78	260^{+170}_{-90}	$1.9^{+1.8}_{-0.1}$	0.53	⋯	⋯
	20	19	$0.3899^{+0.0003}_{-0.0003}$	$147.8424^{+0.0052}_{-0.0055}$	$26.5783^{+0.0090}_{-0.0077}$	0.55	240^{+40}_{-40}	$1.5^{+0.7}_{-0.5}$	0.48	⋯	⋯

Table 1
(Continued)

Field	Group	N_m	z_{grp}	$\overline{\text{R.A.}}$ (deg)	$\overline{\text{Decl.}}$ (deg)	R[b] (′)	σ_{grp} (km s^{-1})	M_{vir}[c] ($10^{13}\,M_\odot$)	r_{vir} (Mpc)	Flag[d]	Match[e]
	21	5	$0.4090^{+0.0011}_{-0.0001}$	$147.8187^{+0.0118}_{-0.0112}$	$26.6435^{+0.0083}_{-0.0070}$	3.64	140^{+110}_{-3}	$\cdots$	0.28	$\cdots$	$\cdots$
	23	6	$0.4484^{+0.0008}_{-0.0007}$	$147.8056^{+0.0222}_{-0.0241}$	$26.4905^{+0.0110}_{-0.0111}$	6.16	400^{+60}_{-250}	$5.7^{+2.4}_{-4.1}$	0.77	$\cdots$	$\cdots$
	24	9	$0.4562^{+0.0006}_{-0.0007}$	$147.9445^{+0.0192}_{-0.0174}$	$26.5534^{+0.0133}_{-0.0131}$	5.75	340^{+60}_{-120}	$3.6^{+1.9}_{-2.2}$	0.66	$\cdots$	$\cdots$
	25	5	$0.5449^{+0.0007}_{-0.0006}$	$147.8640^{+0.0090}_{-0.0092}$	$26.4582^{+0.0039}_{-0.0039}$	7.82	220^{+40}_{-80}	$1.0^{+0.5}_{-0.5}$	0.40	$\cdots$	$\cdots$
	26	9	$0.5553^{+0.0008}_{-0.0007}$	$147.6640^{+0.0075}_{-0.0067}$	$26.4931^{+0.0166}_{-0.0172}$	11.20	400^{+70}_{-160}	$5.5^{+2.6}_{-3.6}$	0.74	4	$\cdots$
	27	5	$0.5610^{+0.0017}_{-0.0008}$	$147.7251^{+0.0124}_{-0.0099}$	$26.5722^{+0.0109}_{-0.0109}$	6.45	430^{+110}_{-340}	$6.7^{+4.4}_{-4.2}$	0.79	4	$\cdots$
	28	9	$0.6393^{+0.0007}_{-0.0007}$	$147.9528^{+0.0093}_{-0.0091}$	$26.7530^{+0.0080}_{-0.0073}$	11.53	270^{+60}_{-160}	$1.7^{+1.0}_{-1.1}$	0.47	$\cdots$	$\cdots$
	29	6	$0.6424^{+0.0007}_{-0.0008}$	$147.8988^{+0.0102}_{-0.0097}$	$26.6415^{+0.0052}_{-0.0054}$	4.38	370^{+80}_{-120}	$4.2^{+2.5}_{-2.3}$	0.65	$\cdots$	$\cdots$
	30	9	$0.6628^{+0.0008}_{-0.0008}$	$147.8644^{+0.0144}_{-0.0163}$	$26.6661^{+0.0071}_{-0.0080}$	4.85	370^{+90}_{-150}	$4.0^{+2.7}_{-2.3}$	0.63	$\cdots$	$\cdots$
h1413	0	6	$0.1378^{+0.0004}_{-0.0006}$	$214.0646^{+0.0280}_{-0.0301}$	$11.3451^{+0.0365}_{-0.0349}$	11.52	330^{+70}_{-180}	$4.0^{+2.2}_{-2.4}$	0.75	3	$\cdots$
	1	7	$0.1542^{+0.0003}_{-0.0004}$	$213.9008^{+0.0288}_{-0.0261}$	$11.5907^{+0.0281}_{-0.0261}$	6.23	220^{+50}_{-130}	$1.4^{+0.8}_{-1.0}$	0.51	$\cdots$	$\cdots$
	2	22	$0.2544^{+0.0005}_{-0.0005}$	$213.8083^{+0.0220}_{-0.0197}$	$11.4769^{+0.0197}_{-0.0197}$	7.98	460^{+40}_{-40}	$9.4^{+2.4}_{-2.2}$	1.00	3	$\cdots$
h12531	0	22	$0.0531^{+0.0007}_{-0.0008}$	$193.4455^{+0.0267}_{-0.0284}$	$-29.1569^{+0.0186}_{-0.0202}$	10.15	980^{+170}_{-170}	$83.4^{+43.2}_{-32.0}$	2.34	1, 2, 3	KSG
	2	6	$0.2461^{+0.0005}_{-0.0007}$	$193.1684^{+0.0351}_{-0.0310}$	$-29.3844^{+0.0227}_{-0.0234}$	10.30	300^{+60}_{-200}	$3.0^{+1.6}_{-2.0}$	0.66	3	$\cdots$
	3	5	$0.2611^{+0.0007}_{-0.0008}$	$193.4756^{+0.0147}_{-0.0147}$	$-29.3344^{+0.0161}_{-0.0161}$	11.75	300^{+80}_{-170}	$2.9^{+2.0}_{-1.9}$	0.65	3	$\cdots$
	4	6	$0.3938^{+0.0004}_{-0.0010}$	$193.2461^{+0.0255}_{-0.0263}$	$-29.2639^{+0.0075}_{-0.0075}$	2.13	360^{+90}_{-220}	$4.6^{+2.4}_{-2.0}$	0.73	$\cdots$	$\cdots$
	7	5	$0.7446^{+0.0006}_{-0.0010}$	$193.2672^{+0.0086}_{-0.0105}$	$-29.4489^{+0.0083}_{-0.0080}$	12.45	330^{+80}_{-60}	$3.0^{+1.9}_{-1.0}$	0.55	3	$\cdots$
he0435	0	9	$0.0503^{+0.0002}_{-0.0002}$	$69.5780^{+0.0275}_{-0.0282}$	$-12.3299^{+0.0253}_{-0.0218}$	2.72	150^{+30}_{-30}	$\cdots$	0.35	1, 2	$\cdots$
	1	11	$0.1844^{+0.0015}_{-0.0010}$	$69.5771^{+0.0297}_{-0.0345}$	$-12.2859^{+0.0248}_{-0.0240}$	0.89	810^{+190}_{-440}	$46.0^{+31.0}_{-30.8}$	1.81	2	$\cdots$
	2	5	$0.3205^{+0.0003}_{-0.0003}$	$69.7469^{+0.0114}_{-0.0114}$	$-12.3235^{+0.0130}_{-0.0157}$	11.05	200^{+40}_{-50}	$1.0^{+0.5}_{-0.4}$	0.42	$\cdots$	$\cdots$
	5[a]	12	$0.4550^{+0.0007}_{-0.0007}$	$69.5521^{+0.0107}_{-0.0129}$	$-12.2839^{+0.0109}_{-0.0109}$	0.61	520^{+80}_{-90}	$11.7^{+5.2}_{-4.3}$	1.01	$\cdots$	$\cdots$
	7	15	$0.5056^{+0.0008}_{-0.0007}$	$69.5731^{+0.0086}_{-0.0091}$	$-12.2211^{+0.0119}_{-0.0123}$	4.03	470^{+70}_{-90}	$8.9^{+3.5}_{-3.4}$	0.89	4	$\cdots$
	8	9	$0.5066^{+0.0009}_{-0.0010}$	$69.7186^{+0.0081}_{-0.0088}$	$-12.2772^{+0.0157}_{-0.0134}$	9.21	400^{+70}_{-190}	$5.6^{+3.0}_{-4.3}$	0.75	4	$\cdots$
	9	6	$0.5554^{+0.0010}_{-0.0013}$	$69.5506^{+0.0113}_{-0.0163}$	$-12.3312^{+0.0112}_{-0.0124}$	2.71	360^{+60}_{-290}	$4.3^{+1.9}_{-3.0}$	0.67	$\cdots$	$\cdots$
he1104	0	10	$0.1317^{+0.0017}_{-0.0015}$	$166.6834^{+0.0392}_{-0.0409}$	$-18.3403^{+0.0240}_{-0.0235}$	2.72	1100^{+210}_{-250}	$111.1^{+62.2}_{-48.8}$	2.54	2	$\cdots$
	1	13	$0.1524^{+0.0010}_{-0.0006}$	$166.6619^{+0.0322}_{-0.0316}$	$-18.4703^{+0.0171}_{-0.0191}$	6.94	500^{+130}_{-200}	$12.3^{+9.9}_{-7.6}$	1.13	3	$\cdots$
	2	23	$0.2162^{+0.0005}_{-0.0005}$	$166.6853^{+0.0256}_{-0.0252}$	$-18.4000^{+0.0205}_{-0.0194}$	3.71	520^{+60}_{-70}	$13.4^{+4.6}_{-4.4}$	1.15	$\cdots$	$\cdots$
	3	5	$0.3485^{+0.0003}_{-0.0003}$	$166.4900^{+0.0048}_{-0.0051}$	$-18.2781^{+0.0064}_{-0.0064}$	9.70	160^{+30}_{-40}	$\cdots$	0.33	$\cdots$	$\cdots$
	4	5	$0.4824^{+0.0004}_{-0.0015}$	$166.5071^{+0.0077}_{-0.0092}$	$-18.3104^{+0.0092}_{-0.0092}$	8.00	320^{+210}_{-50}	$3.2^{+2.6}_{-0.1}$	0.62	$\cdots$	$\cdots$
	5	8	$0.4912^{+0.0006}_{-0.0005}$	$166.4846^{+0.0126}_{-0.0127}$	$-18.4961^{+0.0063}_{-0.0077}$	12.13	320^{+60}_{-100}	$3.0^{+1.4}_{-1.4}$	0.60	3	$\cdots$
	6	18	$0.4906^{+0.0015}_{-0.0007}$	$166.7083^{+0.0160}_{-0.0166}$	$-18.3189^{+0.0160}_{-0.0164}$	4.56	600^{+70}_{-80}	$17.0^{+5.6}_{-5.5}$	1.14	$\cdots$	$\cdots$
	7	7	$0.5077^{+0.0008}_{-0.0008}$	$166.7403^{+0.0134}_{-0.0152}$	$-18.5096^{+0.0043}_{-0.0047}$	10.84	400^{+90}_{-190}	$5.6^{+3.6}_{-3.5}$	0.75	$\cdots$	$\cdots$
	9	7	$0.5156^{+0.0005}_{-0.0004}$	$166.5476^{+0.0098}_{-0.0115}$	$-18.4656^{+0.0105}_{-0.0117}$	8.35	310^{+100}_{-180}	$2.9^{+2.7}_{-1.8}$	0.59	$\cdots$	$\cdots$
	10	5	$0.5178^{+0.0006}_{-0.0004}$	$166.5965^{+0.0022}_{-0.0022}$	$-18.3297^{+0.0056}_{-0.0056}$	2.90	180^{+30}_{-40}	$\cdots$	0.34	$\cdots$	$\cdots$
	11	14	$0.5327^{+0.0011}_{-0.0008}$	$166.5140^{+0.0222}_{-0.0218}$	$-18.3208^{+0.0089}_{-0.0091}$	7.43	660^{+120}_{-170}	$22.0^{+11.3}_{-10.3}$	1.23	$\cdots$	$\cdots$
	12	7	$0.5388^{+0.0013}_{-0.0012}$	$166.6961^{+0.0103}_{-0.0086}$	$-18.5160^{+0.0124}_{-0.0116}$	10.10	530^{+100}_{-170}	$11.7^{+5.7}_{-6.0}$	0.98	3	$\cdots$
he2149	0	5	$0.0937^{+0.0002}_{-0.0005}$	$328.0581^{+0.0154}_{-0.0154}$	$-27.5883^{+0.0233}_{-0.0233}$	3.76	130^{+90}_{-30}	$\cdots$	0.30	1, 3	$\cdots$
	1	13	$0.2736^{+0.0006}_{-0.0004}$	$328.0089^{+0.0073}_{-0.0085}$	$-27.5268^{+0.0052}_{-0.0053}$	1.21	330^{+50}_{-50}	$3.6^{+1.5}_{-1.2}$	0.70	3	$\cdots$
	2	7	$0.4454^{+0.0005}_{-0.0008}$	$328.0657^{+0.0146}_{-0.0172}$	$-27.5237^{+0.0080}_{-0.0066}$	1.88	340^{+80}_{-200}	$3.7^{+2.4}_{-2.5}$	0.66	3	WMKZL06
hst14113	0	26	$0.0808^{+0.0008}_{-0.0008}$	$212.7726^{+0.0394}_{-0.0394}$	$52.2633^{+0.0280}_{-0.0293}$	4.82	1000^{+120}_{-130}	$86.5^{+29.7}_{-26.2}$	2.35	1, 2	MNR05
	1	8	$0.1954^{+0.0006}_{-0.0006}$	$212.9422^{+0.0565}_{-0.0585}$	$52.2274^{+0.0355}_{-0.0312}$	4.59	380^{+80}_{-120}	$5.8^{+3.3}_{-2.9}$	0.85	$\cdots$	$\cdots$
	2	9	$0.2351^{+0.0006}_{-0.0007}$	$212.8764^{+0.0206}_{-0.0189}$	$52.2789^{+0.0205}_{-0.0219}$	5.48	370^{+80}_{-110}	$5.4^{+3.2}_{-2.7}$	0.82	$\cdots$	$\cdots$
	3	19	$0.2705^{+0.0005}_{-0.0005}$	$212.8348^{+0.0479}_{-0.0411}$	$52.2320^{+0.0129}_{-0.0127}$	2.42	500^{+70}_{-70}	$11.7^{+4.5}_{-3.6}$	1.07	$\cdots$	$\cdots$
	7	5	$0.3622^{+0.0006}_{-0.0005}$	$212.9963^{+0.0213}_{-0.0202}$	$52.3031^{+0.0146}_{-0.0143}$	9.01	220^{+60}_{-70}	$1.1^{+1.0}_{-0.7}$	0.44	$\cdots$	$\cdots$
	8	7	$0.4504^{+0.0009}_{-0.0012}$	$212.8249^{+0.0078}_{-0.0045}$	$52.2078^{+0.0044}_{-0.0045}$	1.00	410^{+80}_{-230}	$6.2^{+3.5}_{-4.3}$	0.80	$\cdots$	$\cdots$
	9	6	$0.4592^{+0.0004}_{-0.0003}$	$212.6862^{+0.0152}_{-0.0138}$	$52.2638^{+0.0066}_{-0.0066}$	6.89	180^{+40}_{-150}	$\cdots$	0.35	$\cdots$	DG92
	10[a]	55	$0.4603^{+0.0003}_{-0.0003}$	$212.8659^{+0.0103}_{-0.0099}$	$52.1385^{+0.0091}_{-0.0091}$	3.42	500^{+40}_{-40}	$10.9^{+2.3}_{-2.4}$	0.98	4	DG92
	11	11	$0.4823^{+0.0006}_{-0.0007}$	$212.6672^{+0.0163}_{-0.0207}$	$52.3392^{+0.0195}_{-0.0175}$	10.73	430^{+80}_{-90}	$7.2^{+3.7}_{-3.0}$	0.83	$\cdots$	$\cdots$
	12	6	$0.4828^{+0.0005}_{-0.0006}$	$212.9251^{+0.0201}_{-0.0207}$	$52.1613^{+0.0100}_{-0.0098}$	3.88	300^{+70}_{-70}	$2.5^{+1.5}_{-1.1}$	0.57	$\cdots$	$\cdots$
	13	6	$0.4841^{+0.0003}_{-0.0003}$	$212.9074^{+0.0146}_{-0.0125}$	$52.2818^{+0.0088}_{-0.0084}$	6.08	170^{+40}_{-90}	$\cdots$	0.32	$\cdots$	$\cdots$
	15	6	$0.5711^{+0.0006}_{-0.0004}$	$212.8798^{+0.0082}_{-0.0083}$	$52.1938^{+0.0047}_{-0.0052}$	1.76	220^{+50}_{-90}	$1.1^{+0.6}_{-0.5}$	0.41	$\cdots$	$\cdots$
lbq1333	0	10	$0.0789^{+0.0002}_{-0.0002}$	$203.7301^{+0.0202}_{-0.0200}$	$1.3404^{+0.0105}_{-0.0115}$	10.16	200^{+30}_{-40}	$1.0^{+0.5}_{-0.4}$	0.47	1, 3	$\cdots$
	1	5	$0.0856^{+0.0003}_{-0.0003}$	$203.7044^{+0.0270}_{-0.0247}$	$1.2053^{+0.0397}_{-0.0544}$	12.81	190^{+40}_{-70}	$\cdots$	0.44	1, 3	MPES09
	2	6	$0.1251^{+0.0002}_{-0.0002}$	$203.8371^{+0.0202}_{-0.0188}$	$1.3506^{+0.0111}_{-0.0095}$	4.55	120^{+20}_{-30}	$\cdots$	0.27	$\cdots$	$\cdots$
	3	5	$0.1420^{+0.0003}_{-0.0005}$	$203.6862^{+0.0069}_{-0.0069}$	$1.2971^{+0.0444}_{-0.0444}$	12.53	220^{+60}_{-40}	$1.4^{+1.1}_{-0.5}$	0.51	3	$\cdots$
	4	36	$0.2422^{+0.0004}_{-0.0004}$	$203.9447^{+0.0191}_{-0.0185}$	$1.2444^{+0.0114}_{-0.0124}$	4.54	550^{+50}_{-50}	$15.9^{+4.3}_{-3.7}$	1.21	$\cdots$	$\cdots$
	7	5	$0.4055^{+0.0016}_{-0.0009}$	$203.8209^{+0.0140}_{-0.0140}$	$1.3515^{+0.0091}_{-0.0091}$	5.36	480^{+60}_{-100}	$10.0^{+3.8}_{-4.6}$	0.97	$\cdots$	$\cdots$

Table 1
(Continued)

Field	Group	N_m	z_{grp}	$\overline{R.A.}$ (deg)	$\overline{Decl.}$ (deg)	R^b (′)	σ_{grp} (km s^{-1})	M_{vir}^c ($10^{13}\,M_\odot$)	r_{vir} (Mpc)	Flag[d]	Match[e]
	8	5	$0.4751^{+0.0007}_{-0.0004}$	$203.9846^{+0.0095}_{-0.0091}$	$1.3566^{+0.0088}_{-0.0073}$	6.31	200^{+40}_{-70}	⋯	0.38	⋯	⋯
	9	9	$0.5710^{+0.0005}_{-0.0004}$	$204.0580^{+0.0088}_{-0.0100}$	$1.3495^{+0.0113}_{-0.0121}$	10.19	310^{+70}_{-80}	$2.6^{+1.8}_{-1.2}$	0.56	3	⋯
mg0751	1	6	$0.2479^{+0.0002}_{-0.0003}$	$117.8481^{+0.0190}_{-0.0184}$	$27.3151^{+0.0080}_{-0.0086}$	4.64	150^{+40}_{-40}	⋯	0.33	⋯	⋯
	2[a]	26	$0.3501^{+0.0003}_{-0.0003}$	$117.9100^{+0.0103}_{-0.0112}$	$27.2903^{+0.0090}_{-0.0089}$	1.12	400^{+60}_{-70}	$6.1^{+2.9}_{-2.5}$	0.82	⋯	WMKZL06
	3	13	$0.5597^{+0.0004}_{-0.0004}$	$117.9046^{+0.0083}_{-0.0093}$	$27.2777^{+0.0072}_{-0.0082}$	0.98	310^{+60}_{-70}	$2.7^{+1.5}_{-1.2}$	0.57	⋯	WMKZL06
mg1131	0	11	$0.0681^{+0.0015}_{-0.0014}$	$172.9282^{+0.0372}_{-0.0361}$	$4.9222^{+0.0444}_{-0.0425}$	3.45	1200^{+150}_{-240}	$144.4^{+51.9}_{-61.9}$	2.84	1, 2	⋯
	1	6	$0.0864^{+0.0006}_{-0.0010}$	$172.8050^{+0.0257}_{-0.0268}$	$4.9138^{+0.0534}_{-0.0504}$	10.82	410^{+80}_{-330}	$7.5^{+3.8}_{-5.1}$	0.97	1, 3	⋯
	2	7	$0.1083^{+0.0005}_{-0.0009}$	$172.9744^{+0.0596}_{-0.0564}$	$4.7648^{+0.0358}_{-0.0386}$	9.96	350^{+70}_{-120}	$4.7^{+2.5}_{-2.5}$	0.81	⋯	⋯
	3	5	$0.1647^{+0.0003}_{-0.0004}$	$173.0796^{+0.0154}_{-0.0159}$	$5.1456^{+0.0195}_{-0.0172}$	14.09	190^{+40}_{-70}	⋯	0.44	⋯	⋯
	5	9	$0.2352^{+0.0005}_{-0.0005}$	$172.9635^{+0.0227}_{-0.0209}$	$4.9339^{+0.0248}_{-0.0214}$	1.32	300^{+50}_{-240}	$3.0^{+1.3}_{-2.3}$	0.66	⋯	⋯
	6	5	$0.2695^{+0.0003}_{-0.0004}$	$172.9150^{+0.0037}_{-0.0037}$	$4.7196^{+0.0186}_{-0.0215}$	13.33	160^{+40}_{-110}	⋯	0.34	⋯	⋯
	7	9	$0.3173^{+0.0008}_{-0.0006}$	$173.1652^{+0.0182}_{-0.0172}$	$4.8401^{+0.0152}_{-0.0129}$	12.04	380^{+70}_{-160}	$5.5^{+2.7}_{-3.0}$	0.80	⋯	⋯
	8	38	$0.3424^{+0.0005}_{-0.0006}$	$172.9286^{+0.0144}_{-0.0143}$	$4.8829^{+0.0144}_{-0.0151}$	4.43	700^{+70}_{-80}	$29.0^{+8.4}_{-7.5}$	1.45	⋯	⋯
mg1549	0	7	$0.0709^{+0.0001}_{-0.0001}$	$237.1965^{+0.0134}_{-0.0147}$	$30.5059^{+0.0092}_{-0.0083}$	17.77	60^{+10}_{-20}	⋯	0.15	1, 3	LCKJ09
	1	11	$0.1574^{+0.0011}_{-0.0006}$	$237.2557^{+0.0498}_{-0.0530}$	$30.7527^{+0.0352}_{-0.0385}$	3.17	490^{+90}_{-120}	$11.7^{+6.1}_{-5.5}$	1.11	⋯	⋯
	2	5	$0.2145^{+0.0001}_{-0.0004}$	$237.1809^{+0.0096}_{-0.0096}$	$30.9320^{+0.0078}_{-0.0078}$	10.64	210^{+60}_{-110}	$1.1^{+0.9}_{-0.7}$	0.47	⋯	⋯
	6	12	$0.3405^{+0.0010}_{-0.0005}$	$237.3018^{+0.0208}_{-0.0208}$	$30.5277^{+0.0117}_{-0.0105}$	15.61	350^{+50}_{-240}	$4.4^{+1.7}_{-3.2}$	0.73	3	⋯
	7	6	$0.3487^{+0.0005}_{-0.0003}$	$237.1503^{+0.0170}_{-0.0132}$	$30.7489^{+0.0116}_{-0.0097}$	8.14	220^{+50}_{-90}	$1.2^{+0.8}_{-0.7}$	0.45	⋯	⋯
	8	9	$0.3587^{+0.0004}_{-0.0004}$	$237.2439^{+0.0134}_{-0.0144}$	$30.6908^{+0.0147}_{-0.0162}$	6.54	280^{+60}_{-90}	$2.4^{+1.5}_{-1.3}$	0.58	⋯	⋯
	9	8	$0.6563^{+0.0011}_{-0.0011}$	$237.3534^{+0.0226}_{-0.0231}$	$30.6912^{+0.0101}_{-0.0095}$	6.39	550^{+110}_{-150}	$12.5^{+6.8}_{-6.0}$	0.96	⋯	⋯
mg1654	0	24	$0.1233^{+0.0005}_{-0.0005}$	$253.7029^{+0.0197}_{-0.0197}$	$13.7101^{+0.0149}_{-0.0155}$	4.11	580^{+90}_{-80}	$18.8^{+8.6}_{-5.7}$	1.33	2	⋯
	1	5	$0.1517^{+0.0003}_{-0.0002}$	$253.8286^{+0.0248}_{-0.0248}$	$13.7301^{+0.0058}_{-0.0055}$	9.35	180^{+50}_{-40}	⋯	0.41	⋯	⋯
	2	5	$0.1732^{+0.0002}_{-0.0005}$	$253.7528^{+0.0102}_{-0.0103}$	$13.6062^{+0.0176}_{-0.0173}$	10.99	160^{+30}_{-30}	⋯	0.36	3	⋯
	3[a]	8	$0.2520^{+0.0002}_{-0.0002}$	$253.6644^{+0.0050}_{-0.0052}$	$13.7884^{+0.0067}_{-0.0067}$	1.10	160^{+40}_{-40}	⋯	0.36	⋯	WMKZL06
	4	19	$0.2797^{+0.0009}_{-0.0007}$	$253.6344^{+0.0185}_{-0.0180}$	$13.7546^{+0.0213}_{-0.0218}$	2.57	810^{+130}_{-160}	$44.0^{+21.5}_{-18.3}$	1.73	⋯	⋯
	5	13	$0.3265^{+0.0007}_{-0.0006}$	$253.7769^{+0.0157}_{-0.0151}$	$13.6830^{+0.0197}_{-0.0214}$	8.05	480^{+80}_{-90}	$10.5^{+5.1}_{-4.0}$	1.01	⋯	⋯
	6	7	$0.3662^{+0.0015}_{-0.0012}$	$253.7516^{+0.0050}_{-0.0089}$	$13.7505^{+0.0070}_{-0.0089}$	4.70	500^{+130}_{-350}	$11.3^{+7.1}_{-6.0}$	1.02	⋯	⋯
	7	9	$0.3792^{+0.0005}_{-0.0004}$	$253.6941^{+0.0160}_{-0.0152}$	$13.7766^{+0.0120}_{-0.0119}$	1.18	310^{+180}_{-150}	$3.0^{+4.3}_{-0.8}$	0.63	⋯	⋯
	9	8	$0.5719^{+0.0007}_{-0.0007}$	$253.5471^{+0.0127}_{-0.0141}$	$13.8332^{+0.0049}_{-0.0056}$	8.25	320^{+60}_{-150}	$2.9^{+1.5}_{-1.8}$	0.58	⋯	⋯
	10	5	$0.7129^{+0.0009}_{-0.0015}$	$253.6238^{+0.0102}_{-0.0095}$	$13.7121^{+0.0095}_{-0.0095}$	4.68	450^{+70}_{-380}	$6.9^{+2.9}_{-4.6}$	0.76	⋯	⋯
pg1115	1	8	$0.0418^{+0.0001}_{-0.0001}$	$169.5271^{+0.0286}_{-0.0257}$	$7.7177^{+0.0187}_{-0.0174}$	3.90	100^{+20}_{-30}	⋯	0.23	1	⋯
	2	6	$0.0746^{+0.0002}_{-0.0003}$	$169.6817^{+0.0411}_{-0.0409}$	$7.9842^{+0.0200}_{-0.0198}$	14.65	130^{+80}_{-40}	⋯	0.31	1, 3	⋯
	3	10	$0.1057^{+0.0005}_{-0.0003}$	$169.6727^{+0.0168}_{-0.0190}$	$7.7496^{+0.0469}_{-0.0510}$	6.15	330^{+80}_{-90}	$4.1^{+2.6}_{-1.8}$	0.77	⋯	⋯
	4	11	$0.1600^{+0.0006}_{-0.0007}$	$169.4178^{+0.0293}_{-0.0249}$	$7.7690^{+0.0146}_{-0.0140}$	9.09	520^{+90}_{-100}	$14.0^{+6.6}_{-5.3}$	1.18	3	MB
	5	16	$0.2249^{+0.0003}_{-0.0004}$	$169.5240^{+0.0170}_{-0.0185}$	$7.7609^{+0.0119}_{-0.0116}$	2.79	350^{+80}_{-80}	$4.5^{+3.1}_{-2.1}$	0.77	⋯	⋯
	6[a]	13	$0.3097^{+0.0005}_{-0.0005}$	$169.5681^{+0.0060}_{-0.0065}$	$7.7648^{+0.0042}_{-0.0044}$	0.17	390^{+50}_{-60}	$5.8^{+2.3}_{-2.1}$	0.82	⋯	WMKZL06
	7	20	$0.4819^{+0.0007}_{-0.0006}$	$169.3732^{+0.0090}_{-0.0079}$	$7.7326^{+0.0040}_{-0.0044}$	11.91	530^{+70}_{-70}	$12.4^{+4.7}_{-3.9}$	1.02	3	CCN07
	8	11	$0.4859^{+0.0004}_{-0.0004}$	$169.5726^{+0.0075}_{-0.0079}$	$7.7769^{+0.0045}_{-0.0048}$	0.65	210^{+40}_{-60}	$1.0^{+0.5}_{-0.5}$	0.40	⋯	WH
	9	5	$0.4922^{+0.0007}_{-0.0005}$	$169.3634^{+0.0077}_{-0.0077}$	$7.7173^{+0.0044}_{-0.0044}$	12.67	300^{+60}_{-110}	$2.5^{+1.2}_{-1.4}$	0.57	3	CCN07
	11	5	$0.4992^{+0.0007}_{-0.0006}$	$169.5150^{+0.0140}_{-0.0139}$	$7.7324^{+0.0051}_{-0.0052}$	3.88	300^{+190}_{-170}	$2.5^{+3.6}_{-0.5}$	0.56	⋯	⋯
q0047	1	29	$0.1952^{+0.0004}_{-0.0004}$	$12.4432^{+0.0214}_{-0.0209}$	$-27.8796^{+0.0133}_{-0.0134}$	1.05	490^{+70}_{-70}	$11.3^{+4.9}_{-3.8}$	1.08	⋯	⋯
	2	6	$0.2379^{+0.0003}_{-0.0005}$	$12.2687^{+0.0277}_{-0.0282}$	$-27.8515^{+0.0065}_{-0.0067}$	8.37	210^{+70}_{-130}	$1.0^{+1.0}_{-0.5}$	0.45	3	⋯
	3	14	$0.3081^{+0.0003}_{-0.0003}$	$12.3197^{+0.0169}_{-0.0165}$	$-27.9351^{+0.0091}_{-0.0094}$	6.66	340^{+70}_{-70}	$4.2^{+2.5}_{-1.6}$	0.73	⋯	⋯
	5	5	$0.3748^{+0.0008}_{-0.0009}$	$12.2895^{+0.0181}_{-0.0081}$	$-27.9852^{+0.0081}_{-0.0081}$	9.79	250^{+230}_{-4}	$1.6^{+1.6}_{-0.0003}$	0.50	3	⋯
	6[a]	20	$0.4890^{+0.0007}_{-0.0008}$	$12.4834^{+0.0176}_{-0.0160}$	$-27.8511^{+0.0095}_{-0.0095}$	3.41	630^{+70}_{-80}	$20.0^{+6.4}_{-5.7}$	1.21	⋯	⋯
	7	8	$0.5375^{+0.0004}_{-0.0003}$	$12.4062^{+0.0070}_{-0.0062}$	$-27.8631^{+0.0067}_{-0.0074}$	1.17	180^{+40}_{-60}	⋯	0.33	⋯	⋯
	8	5	$0.5963^{+0.0007}_{-0.0008}$	$12.3682^{+0.0108}_{-0.0108}$	$-27.8974^{+0.0013}_{-0.0013}$	3.30	180^{+50}_{-80}	⋯	0.33	⋯	⋯
	9	5	$0.6533^{+0.0004}_{-0.0003}$	$12.4317^{+0.0073}_{-0.0077}$	$-27.8765^{+0.0065}_{-0.0065}$	0.41	170^{+30}_{-40}	⋯	0.30	⋯	⋯
q0158	0	19	$0.2917^{+0.0009}_{-0.0008}$	$29.7448^{+0.0320}_{-0.0360}$	$-43.3772^{+0.0166}_{-0.0145}$	3.97	820^{+110}_{-120}	$45.6^{+17.9}_{-15.1}$	1.75	2	⋯
	2	5	$0.4249^{+0.0003}_{-0.0002}$	$29.6714^{+0.0081}_{-0.0081}$	$-43.3836^{+0.0112}_{-0.0112}$	2.05	220^{+40}_{-160}	$1.2^{+0.6}_{-0.8}$	0.44	⋯	⋯
	3	5	$0.5364^{+0.0006}_{-0.0009}$	$29.6557^{+0.0098}_{-0.0151}$	$-43.3912^{+0.0080}_{-0.0080}$	1.75	310^{+70}_{-190}	$2.8^{+1.8}_{-2.1}$	0.58	⋯	⋯
	4	6	$0.6783^{+0.0011}_{-0.0009}$	$29.6649^{+0.0059}_{-0.0078}$	$-43.3841^{+0.0012}_{-0.0012}$	2.05	420^{+80}_{-120}	$6.0^{+3.0}_{-2.8}$	0.73	⋯	⋯
q1017	0	5	$0.2479^{+0.0022}_{-0.0002}$	$154.1780^{+0.0260}_{-0.0260}$	$-20.7539^{+0.0110}_{-0.0110}$	9.79	460^{+410}_{-40}	$9.5^{+9.4}_{-0.02}$	1.00	3	⋯
	1	49	$0.2576^{+0.0005}_{-0.0004}$	$154.3972^{+0.0120}_{-0.0118}$	$-20.9111^{+0.0132}_{-0.0127}$	8.14	620^{+70}_{-80}	$21.5^{+6.7}_{-6.2}$	1.34	3	⋯
	2	13	$0.2848^{+0.0005}_{-0.0004}$	$154.3842^{+0.0198}_{-0.0192}$	$-20.7645^{+0.0092}_{-0.0099}$	2.23	280^{+40}_{-100}	$2.4^{+1.1}_{-1.5}$	0.60	⋯	⋯
	3	8	$0.2947^{+0.0004}_{-0.0003}$	$154.2215^{+0.0085}_{-0.0085}$	$-20.9374^{+0.0108}_{-0.0108}$	11.73	220^{+40}_{-50}	$1.2^{+0.6}_{-0.5}$	0.47	3	⋯
	4	5	$0.2954^{+0.0007}_{-0.0005}$	$154.5049^{+0.0139}_{-0.0139}$	$-20.7702^{+0.0131}_{-0.0131}$	8.74	340^{+100}_{-250}	$4.2^{+3.1}_{-2.4}$	0.73	⋯	⋯

Table 1
(Continued)

Field	Group	N_m	z_{grp}	$\overline{\text{R.A.}}$ (deg)	$\overline{\text{Decl.}}$ (deg)	R [b] (′)	σ_{grp} (km s^{-1})	M_{vir} [c] ($10^{13}\,M_\odot$)	r_{vir} (Mpc)	Flag [d]	Match [e]
	6	5	$0.3053^{+0.0004}_{-0.0002}$	$154.5353^{+0.0014}_{-0.0015}$	$-20.7279^{+0.0129}_{-0.0129}$	10.92	160^{+30}_{-30}	...	0.33	3	...
	7	5	$0.3618^{+0.0002}_{-0.0005}$	$154.1936^{+0.0111}_{-0.0104}$	$-20.9540^{+0.0025}_{-0.0025}$	13.49	160^{+50}_{-100}	...	0.34	3	...
	9	7	$0.4582^{+0.0006}_{-0.0007}$	$154.5217^{+0.0117}_{-0.0119}$	$-20.9204^{+0.0093}_{-0.0072}$	12.70	380^{+80}_{-140}	$5.0^{+2.7}_{-2.4}$	0.74	3	...
	10	10	$0.4585^{+0.0007}_{-0.0006}$	$154.2862^{+0.0126}_{-0.0112}$	$-20.7729^{+0.0114}_{-0.0111}$	3.61	380^{+70}_{-100}	$5.2^{+2.9}_{-2.6}$	0.75	...	...
	11	5	$0.4708^{+0.0013}_{-0.0002}$	$154.4132^{+0.0131}_{-0.0111}$	$-20.9513^{+0.0077}_{-0.0076}$	10.71	290^{+260}_{-20}	$2.4^{+2.3}_{-0.005}$	0.56	...	...
	12	5	$0.4723^{+0.0012}_{-0.0011}$	$154.2586^{+0.0111}_{-0.0111}$	$-20.9406^{+0.0129}_{-0.0117}$	10.75	310^{+260}_{-30}	$2.8^{+2.6}_{-0.01}$	0.59	...	...
q1355	0	5	$0.1178^{+0.0013}_{-0.0005}$	$208.9592^{+0.0442}_{-0.0426}$	$-23.0048^{+0.0150}_{-0.0124}$	3.30	340^{+60}_{-190}	$4.5^{+2.2}_{-3.0}$	0.79	2	...
	1	37	$0.1718^{+0.0005}_{-0.0005}$	$209.0153^{+0.0250}_{-0.0220}$	$-22.9736^{+0.0108}_{-0.0108}$	4.78	710^{+100}_{-100}	$32.5^{+13.0}_{-10.2}$	1.60	3	...
	2	5	$0.2175^{+0.0002}_{-0.0004}$	$208.7574^{+0.0105}_{-0.0105}$	$-22.8326^{+0.0024}_{-0.0024}$	12.12	100^{+20}_{-50}	...	0.23	3	...
	3	10	$0.2418^{+0.0003}_{-0.0003}$	$208.8567^{+0.0146}_{-0.0144}$	$-22.9932^{+0.0161}_{-0.0157}$	4.65	200^{+40}_{-40}	$1.0^{+0.5}_{-0.4}$	0.45	...	...
	5	6	$0.2751^{+0.0003}_{-0.0003}$	$208.7203^{+0.0048}_{-0.0052}$	$-23.0295^{+0.0121}_{-0.0120}$	12.43	170^{+40}_{-50}	...	0.36	3	...
	6	10	$0.2772^{+0.0005}_{-0.0005}$	$209.0448^{+0.0146}_{-0.0144}$	$-22.8670^{+0.0069}_{-0.0069}$	8.27	360^{+60}_{-70}	$4.6^{+2.3}_{-1.9}$	0.76	...	...
	7	21	$0.3422^{+0.0008}_{-0.0007}$	$208.9847^{+0.0231}_{-0.0202}$	$-22.9157^{+0.0144}_{-0.0166}$	3.85	770^{+70}_{-70}	$37.9^{+10.1}_{-8.5}$	1.60	3	...
	8	6	$0.3657^{+0.0005}_{-0.0004}$	$208.9153^{+0.0173}_{-0.0170}$	$-22.9515^{+0.0138}_{-0.0139}$	0.91	270^{+60}_{-150}	$2.1^{+1.3}_{-1.5}$	0.56	...	...
	9	6	$0.5561^{+0.0009}_{-0.0008}$	$208.8433^{+0.0166}_{-0.0173}$	$-22.9967^{+0.0086}_{-0.0075}$	5.41	360^{+70}_{-110}	$4.2^{+2.1}_{-2.1}$	0.67	...	...
	10	7	$0.5579^{+0.0006}_{-0.0005}$	$208.8223^{+0.0041}_{-0.0043}$	$-22.8405^{+0.0071}_{-0.0080}$	9.18	210^{+50}_{-100}	$1.0^{+0.6}_{-0.6}$	0.39	3	...
rxj1131	0	5	$0.0531^{+0.0007}_{-0.0003}$	$172.9119^{+0.0074}_{-0.0073}$	$-12.4701^{+0.0437}_{-0.0430}$	4.87	170^{+40}_{-130}	...	0.41	1, 3	TOH00
	1	6	$0.0785^{+0.0009}_{-0.0005}$	$172.9524^{+0.0613}_{-0.0552}$	$-12.5111^{+0.0271}_{-0.0291}$	1.49	560^{+150}_{-320}	$17.4^{+12.3}_{-10.6}$	1.31	1, 2	...
	2	66	$0.1021^{+0.0004}_{-0.0004}$	$172.9579^{+0.0115}_{-0.0115}$	$-12.5501^{+0.0093}_{-0.0082}$	1.10	790^{+90}_{-90}	$45.9^{+14.7}_{-11.9}$	1.85	2	TOH00
	3	7	$0.2822^{+0.0007}_{-0.0004}$	$172.9218^{+0.0348}_{-0.0303}$	$-12.6263^{+0.0173}_{-0.0173}$	6.14	410^{+160}_{-170}	$6.7^{+6.9}_{-2.9}$	0.87	...	...
	4 [a]	38	$0.2938^{+0.0005}_{-0.0005}$	$172.8815^{+0.0137}_{-0.0135}$	$-12.5649^{+0.0081}_{-0.0096}$	5.23	550^{+70}_{-90}	$15.5^{+5.8}_{-5.7}$	1.18	...	WMKZL06
	5	22	$0.3149^{+0.0003}_{-0.0003}$	$172.9963^{+0.0113}_{-0.0115}$	$-12.6234^{+0.0095}_{-0.0088}$	5.74	290^{+30}_{-40}	$2.6^{+0.9}_{-0.8}$	0.61	...	...
	6	15	$0.3232^{+0.0007}_{-0.0005}$	$173.0362^{+0.0173}_{-0.0200}$	$-12.6388^{+0.0087}_{-0.0096}$	7.61	420^{+80}_{-140}	$7.0^{+3.8}_{-4.0}$	0.87	...	...
	8	6	$0.3834^{+0.0006}_{-0.0005}$	$172.9991^{+0.0198}_{-0.0211}$	$-12.5174^{+0.0149}_{-0.0158}$	2.23	360^{+80}_{-120}	$4.5^{+2.5}_{-2.2}$	0.73	...	...
	9	10	$0.4083^{+0.0009}_{-0.0009}$	$172.8362^{+0.0161}_{-0.0139}$	$-12.5290^{+0.0126}_{-0.0123}$	7.52	570^{+80}_{-460}	$15.9^{+5.8}_{-12.5}$	1.14	...	...
	10	8	$0.4246^{+0.0008}_{-0.0005}$	$172.9562^{+0.0123}_{-0.0107}$	$-12.5715^{+0.0128}_{-0.0119}$	2.37	320^{+60}_{-180}	$3.2^{+1.5}_{-2.1}$	0.64	...	...
	12	6	$0.6461^{+0.0010}_{-0.0005}$	$172.8909^{+0.0110}_{-0.0112}$	$-12.6686^{+0.0099}_{-0.0090}$	9.21	320^{+40}_{-220}	$2.9^{+0.9}_{-2.0}$	0.56	...	...
sbs1520	0	13	$0.0853^{+0.0004}_{-0.0003}$	$230.5336^{+0.0611}_{-0.0614}$	$52.9859^{+0.0302}_{-0.0313}$	5.58	260^{+50}_{-70}	$2.1^{+1.3}_{-1.0}$	0.60	1	...
	1	8	$0.1003^{+0.0008}_{-0.0008}$	$230.5330^{+0.0948}_{-0.0853}$	$52.8484^{+0.0567}_{-0.0490}$	5.24	510^{+80}_{-270}	$13.8^{+5.9}_{-10.4}$	1.20	...	...
	2	31	$0.1577^{+0.0007}_{-0.0008}$	$230.4631^{+0.0331}_{-0.0346}$	$52.8460^{+0.0218}_{-0.0219}$	4.16	780^{+90}_{-80}	$42.7^{+14.7}_{-10.7}$	1.78	2	...
	4	29	$0.2043^{+0.0007}_{-0.0008}$	$230.5713^{+0.0334}_{-0.0335}$	$52.9755^{+0.0299}_{-0.0288}$	6.12	970^{+90}_{-110}	$76.5^{+21.4}_{-21.1}$	2.17	3	...
	5	6	$0.2643^{+0.0018}_{-0.0018}$	$230.5162^{+0.0444}_{-0.0481}$	$52.9890^{+0.0118}_{-0.0122}$	5.37	540^{+420}_{-90}	$14.3^{+14.1}_{-0.2}$	1.15	...	...
	6	5	$0.3576^{+0.0011}_{-0.0007}$	$230.3794^{+0.0302}_{-0.0300}$	$53.1965^{+0.0132}_{-0.0132}$	17.11	370^{+90}_{-100}	$5.1^{+3.5}_{-2.3}$	0.77	3	...
	8	6	$0.7590^{+0.0004}_{-0.0006}$	$230.3903^{+0.0064}_{-0.0064}$	$52.9334^{+0.0058}_{-0.0061}$	2.06	210^{+40}_{-160}	...	0.35	...	AFW08
wfi2033	0	7	$0.1740^{+0.0005}_{-0.0007}$	$308.3855^{+0.0563}_{-0.0585}$	$-47.3585^{+0.0287}_{-0.0344}$	2.72	390^{+80}_{-270}	$6.4^{+3.3}_{-4.5}$	0.89	3	...
	2	5	$0.2629^{+0.0007}_{-0.0005}$	$308.2913^{+0.0051}_{-0.0056}$	$-47.2607^{+0.0062}_{-0.0062}$	9.72	250^{+60}_{-80}	$1.7^{+1.0}_{-0.8}$	0.53	3	...
	4	8	$0.4960^{+0.0011}_{-0.0011}$	$308.4254^{+0.0170}_{-0.0170}$	$-47.3846^{+0.0123}_{-0.0144}$	0.64	500^{+90}_{-150}	$10.4^{+5.3}_{-5.7}$	0.95	...	...
	5 [a]	14	$0.6598^{+0.0007}_{-0.0010}$	$308.4475^{+0.0110}_{-0.0107}$	$-47.3668^{+0.0057}_{-0.0060}$	1.94	460^{+60}_{-100}	$7.6^{+2.9}_{-3.5}$	0.80	...	...
	6	5	$0.6838^{+0.0005}_{-0.0004}$	$308.4650^{+0.0113}_{-0.0080}$	$-47.3898^{+0.0062}_{-0.0062}$	1.67	180^{+30}_{-90}	...	0.30	...	...

Notes.

[a] A lens group.

[b] Projected distance between the lens and the group centroid.

[c] Masses are reported when $\geqslant 10^{13}\,M_\odot$.

[d] (1) $z_{grp} < 0.1$ (groups at lower redshift are most likely not sampled out to r_{vir} because of the spectroscopic field size); (2) r_{vir} intersects the edge of the well-sampled region of the field because the group is large and/or at low z; (3) r_{vir} extends beyond the well-sampled region of the field because the group centroid or several of its members are near the edge of the field; (4) group membership was adjusted manually to remedy overlapping membership.

[e] Groups in the literature that have a redshift within $3\sigma_z$ of a group in our catalog. The reference abbreviations are as follows: AFALS07—Auger et al. (2007); AFW08—Auger et al. (2008), CCN07—Carrasco et al. (2007), DG92—Dressler & Gunn (1992), KSG—Katgert et al. (1996), Struble & Rood (1999), and Gastaldello et al. (2003), LCKJ09—Lopes et al. (2009), MB—Mason et al. (2000) and Barkhouse et al. (2006), MPES09—McConnachie et al. (2009), MNR05—Miller et al. (2005), TOH00—Tucker et al. (2000), WMKZL06—Williams et al. (2006), and WH—Williams et al. (2006) and Horner et al. (2008).

standard deviations of the original values using the previously calculated uncertainties, although the effect can be systematic and does not account for groups whose incompleteness would have precluded their identification in the first place. For 25% completeness, the velocity dispersions are underestimated (see Zabludoff & Mulchaey 1998) by a median of 3% and the masses by a median of 9%. We note that the groups with at least 20 members are well sampled and/or rich compared with the other groups in our catalog. The 20+ member groups have a median velocity dispersion of 630 km s^{-1} compared with the median of 350 km s^{-1} for the full sample of 5+ member groups. However, there is considerable overlap in the velocity

Table 2
Group Catalog Supplement: Algorithmically Identified Groups With 3–4 Members

Field	Group	N_m	$z_{\rm grp}$[a]	$\overline{\rm R.A.}$[a] (deg)	$\overline{\rm Decl.}$[a] (deg)	R[b] (′)	$\sigma_{\rm grp}$[a] (km s^{-1})	$M_{\rm vir}$[a,c] ($10^{13}\,M_\odot$)	$r_{\rm vir}$ (Mpc)	Flag[d]	Match[e]
b0712	1	3	0.2635	109.3152	47.0962	12.63	130	⋯	0.28	⋯	⋯
	2	3	0.3483	109.1790	47.1236	6.84	110	⋯	0.22	⋯	⋯
	4	4	$0.3724^{+0.0003}_{-0.0002}$	$109.2126^{+0.0157}_{-0.0158}$	$47.3602^{+0.0166}_{-0.0166}$	15.09	170^{+60}_{-130}	⋯	0.34	⋯	⋯
	6	4	$0.4360^{+0.0004}_{-0.0006}$	$108.9779^{+0.0107}_{-0.0107}$	$47.1869^{+0.0127}_{-0.0127}$	2.82	180^{+30}_{-150}	⋯	0.35	⋯	⋯
b1152	13	3	0.6623	178.9290	19.6922	6.08	110	⋯	0.18	⋯	⋯
b1422	3	3	0.3239	216.1767	22.9344	0.99	100	⋯	0.22	⋯	⋯
	7	4	$0.5706^{+0.0003}_{-0.0006}$	$216.2366^{+0.0044}_{-0.0044}$	$22.7597^{+0.0021}_{-0.0021}$	11.29	170^{+30}_{-90}	⋯	0.32	3	⋯
b1600	5	3	0.2624	240.4598	43.2505	2.51	210	1.1	0.46	⋯	⋯
	6	3	0.2629	240.3343	43.1579	8.19	150	⋯	0.33	⋯	⋯
b2114	1	4	$0.1352^{+0.0002}_{-0.0001}$	$319.1929^{+0.0175}_{-0.0195}$	$2.5600^{+0.0132}_{-0.0157}$	7.90	110^{+20}_{-40}	⋯	0.26	⋯	⋯
	4	4	$0.2992^{+0.0004}_{-0.0004}$	$319.1031^{+0.0068}_{-0.0068}$	$2.5330^{+0.0067}_{-0.0067}$	8.99	220^{+40}_{-60}	$1.2^{+0.7}_{-0.6}$	0.47	⋯	⋯
	6	4	$0.3133^{+0.0002}_{-0.0004}$	$318.9509^{+0.0071}_{-0.0065}$	$2.4709^{+0.0171}_{-0.0171}$	15.83	130^{+20}_{-60}	⋯	0.27	3	⋯
	8	3	0.4061	319.1848	2.4783	3.33	70	⋯	0.14	⋯	⋯
bri0952	3	3	0.3577	148.7067	−1.5036	2.63	110	⋯	0.23	⋯	⋯
fbq0951	13	3	0.3132	148.1107	26.7191	16.34	190	⋯	0.40	3	⋯
	14	3	0.3129	147.7852	26.7560	10.61	80	⋯	0.17	4	⋯
	15	3	0.3142	147.8912	26.6954	6.96	20	⋯	0.03	4	⋯
	16	4	$0.3252^{+0.0003}_{-0.0003}$	$147.6988^{+0.0074}_{-0.0074}$	$26.7918^{+0.0059}_{-0.0059}$	14.54	170^{+20}_{-50}	⋯	0.35	⋯	⋯
	22	3	0.4464	147.5843	26.4793	15.38	230	1.3	0.45	3	⋯
	31	4	$0.6905^{+0.0003}_{-0.0002}$	$147.9302^{+0.0013}_{-0.0014}$	$26.6297^{+0.0029}_{-0.0029}$	5.27	110^{+20}_{-40}	⋯	0.19	⋯	⋯
h1413	3	3	0.3057	213.8439	11.5525	6.74	70	⋯	0.16	⋯	⋯
	4	4	$0.3267^{+0.0007}_{-0.0006}$	$214.0973^{+0.0123}_{-0.0124}$	$11.5402^{+0.0167}_{-0.0187}$	9.48	270^{+50}_{-40}	$2.0^{+0.9}_{-0.5}$	0.56	⋯	⋯
h12531	1	3	0.0817	193.5220	−29.3419	14.12	160	⋯	0.37	1, 3	⋯
	5	4	$0.4505^{+0.0003}_{-0.0003}$	$193.3901^{+0.0129}_{-0.0113}$	$-29.2837^{+0.0081}_{-0.0081}$	6.39	160^{+20}_{-50}	⋯	0.31	⋯	⋯
	6	4	$0.6585^{+0.0002}_{-0.0002}$	$193.2353^{+0.0023}_{-0.0023}$	$-29.1859^{+0.0036}_{-0.0036}$	4.02	80^{+10}_{-40}	⋯	0.15	⋯	⋯
	8	4	$0.7641^{+0.0005}_{-0.0006}$	$193.3045^{+0.0099}_{-0.0099}$	$-29.1943^{+0.0082}_{-0.0099}$	3.17	240^{+40}_{-70}	$1.2^{+0.6}_{-0.6}$	0.39	⋯	⋯
he0435	3	4	$0.3978^{+0.0003}_{-0.0002}$	$69.5680^{+0.0140}_{-0.0140}$	$-12.2930^{+0.0043}_{-0.0043}$	0.49	140^{+20}_{-70}	⋯	0.28	⋯	⋯
	4	4	$0.4186^{+0.0002}_{-0.0002}$	$69.5440^{+0.0057}_{-0.0057}$	$-12.2898^{+0.0018}_{-0.0021}$	1.06	70^{+10}_{-10}	⋯	0.14	⋯	⋯
	6	3	0.4721	69.4977	−12.3741	6.42	80	⋯	0.16	⋯	⋯
he1104	8	4	$0.5147^{+0.0003}_{-0.0003}$	$166.6843^{+0.0054}_{-0.0059}$	$-18.5142^{+0.0041}_{-0.0041}$	9.80	150^{+30}_{-50}	⋯	0.29	⋯	⋯
he2149	3	4	$0.4618^{+0.0006}_{-0.0005}$	$328.0716^{+0.0151}_{-0.0151}$	$-27.5454^{+0.0138}_{-0.0138}$	2.33	260^{+40}_{-100}	$1.7^{+0.9}_{-1.1}$	0.50	⋯	⋯
	4	4	$0.6033^{+0.0002}_{-0.0003}$	$328.0049^{+0.0048}_{-0.0048}$	$-27.5259^{+0.0045}_{-0.0045}$	1.42	130^{+30}_{-120}	⋯	0.24	⋯	WMKZL06
hst14113	4	4	$0.2728^{+0.0008}_{-0.0005}$	$212.9338^{+0.0148}_{-0.0153}$	$51.9318^{+0.0135}_{-0.0135}$	16.03	260^{+40}_{-220}	$2.0^{+0.7}_{-1.3}$	0.56	3	⋯
	5	3	0.2821	212.8434	52.1971	0.53	70	⋯	0.15	⋯	⋯
	6	3	0.3017	213.0337	52.3762	13.32	240	1.5	0.50	⋯	⋯
	14	3	0.5519	212.8167	52.1644	1.73	100	⋯	0.18	⋯	⋯
lbq1333	5	4	$0.2534^{+0.0001}_{-0.0003}$	$204.0324^{+0.0121}_{-0.0121}$	$1.1449^{+0.0101}_{-0.0101}$	12.50	120^{+20}_{-90}	⋯	0.27	3	⋯
	6	3	0.3272	203.7727	1.2878	7.38	160	⋯	0.33	⋯	⋯
mg0751	0	4	$0.0265^{+0.0002}_{-0.0001}$	$117.8839^{+0.0474}_{-0.0474}$	$27.3568^{+0.0316}_{-0.0313}$	5.30	90^{+10}_{-70}	⋯	0.23	1, 2	BHS
	4	4	$0.5845^{+0.0005}_{-0.0005}$	$117.8842^{+0.0085}_{-0.0085}$	$27.2569^{+0.0056}_{-0.0056}$	2.35	210^{+20}_{-40}	⋯	0.38	⋯	⋯
mg1131	4	3	0.2200	172.7875	5.1548	17.92	170	⋯	0.38	3	⋯
mg1549	3	3	0.2726	237.1858	30.7896	5.96	70	⋯	0.16	⋯	⋯
	4	3	0.2857	237.3177	30.6323	9.38	60	⋯	0.13	⋯	⋯
	5	3	0.2866	237.1321	30.8455	9.38	160	⋯	0.34	⋯	⋯
mg1654	8	3	0.4785	253.7666	13.6037	11.48	140	⋯	0.27	⋯	⋯
pg1115	0	4	$0.0369^{+0.0002}_{-0.0002}$	$169.6122^{+0.0721}_{-0.0776}$	$7.5814^{+0.0347}_{-0.0347}$	11.37	110^{+20}_{-60}	⋯	0.28	1, 3	⋯
	10	4	$0.4987^{+0.0003}_{-0.0002}$	$169.3737^{+0.0042}_{-0.0042}$	$7.7400^{+0.0063}_{-0.0063}$	11.81	100^{+20}_{-40}	⋯	0.19	⋯	⋯
q0047	0	4	$0.1184^{+0.0004}_{-0.0002}$	$12.6169^{+0.0290}_{-0.0212}$	$-27.7632^{+0.0298}_{-0.0357}$	12.18	170^{+20}_{-110}	⋯	0.39	3	⋯
	4	4	$0.3263^{+0.0002}_{-0.0003}$	$12.5292^{+0.0152}_{-0.0152}$	$-27.7996^{+0.0104}_{-0.0104}$	7.12	120^{+20}_{-90}	⋯	0.24	⋯	⋯
q0158	1	3	0.4139	29.6006	−43.3657	4.43	200	⋯	0.39	3	⋯
q1017	5	3	0.3028	154.5331	−20.9515	14.43	90	⋯	0.20	3	⋯
	8	4	$0.4311^{+0.0004}_{-0.0006}$	$154.5449^{+0.0171}_{-0.0184}$	$-20.7591^{+0.0060}_{-0.0060}$	11.05	200^{+30}_{-100}	⋯	0.39	⋯	⋯
q1355	4	3	0.2475	208.9193	−22.9612	0.70	130	⋯	0.28	⋯	⋯
rxj1131	7	3	0.3480	173.0612	−12.6816	10.57	130	⋯	0.28	⋯	⋯
	11	3	0.4843	172.8810	−12.5152	5.01	90	⋯	0.18	⋯	⋯
sbs1520	3	4	$0.1924^{+0.0003}_{-0.0004}$	$230.4513^{+0.0243}_{-0.0243}$	$52.7809^{+0.0309}_{-0.0309}$	7.97	200^{+30}_{-140}	$1.0^{+0.5}_{-0.8}$	0.45	⋯	⋯
	7	3	0.4976	230.5159	52.8714	3.82	220	1.1	0.42	⋯	⋯

Table 2
(Continued)

Field	Group	N_m	z_{grp}[a]	$\overline{R.A.}$[a] (deg)	$\overline{Decl.}$[a] (deg)	R[b] (′)	σ_{grp}[a] (km s^{-1})	M_{vir}[a,c] ($10^{13} M_\odot$)	r_{vir} (Mpc)	Flag[d]	Match[e]
wfi2033	1	4	$0.2151^{+0.0005}_{-0.0003}$	$308.5132^{+0.0320}_{-0.0320}$	$-47.3869^{+0.0136}_{-0.0188}$	3.63	210^{+30}_{-30}	$1.1^{+0.4}_{-0.2}$	0.45	⋯	⋯
	3	4	$0.3986^{+0.0004}_{-0.0007}$	$308.1831^{+0.0013}_{-0.0013}$	$-47.3227^{+0.0070}_{-0.0070}$	10.74	250^{+40}_{-120}	$1.6^{+0.7}_{-1.0}$	0.50	3	

Notes.
[a] Uncertainties are not calculated for $N_m < 4$.
[b] Projected distance between the lens and the group centroid.
[c] Masses are reported when $\geqslant 10^{13} M_\odot$.
[d] (1) $z_{grp} < 0.1$ (groups at lower redshift are most likely not sampled out to r_{vir} because of the spectroscopic field size); (2) r_{vir} intersects the edge of the well-sampled region of the field because the group is large and/or at low z; (3) r_{vir} extends beyond the well-sampled region of the field because the group centroid or several of its members are near the edge of the field; (4) group membership was adjusted manually to remedy overlapping membership.
[e] Groups in the literature in these fields that have a redshift within $3\sigma_z$ of a group in our catalog. The reference abbreviations are as follows: BHS—Berlind et al. (2006), Haynes et al. (2011), and Smith et al. (2012); and WMKZL06—Williams et al. (2006).

dispersion ranges of these two samples, 290–1180 km s^{-1} compared with 60–1200 km s^{-1} for the 20+ and 5+ member groups, respectively. More importantly, the systematic offset between the measured velocity dispersion for the full 20+ member groups and for the 25% completeness subsamples does not depend on velocity dispersion; the velocity dispersion is generally underestimated in the 25% subsamples within one standard deviation over the full range of velocity dispersions. Hence, we conclude that the impact of incompleteness, even on the lower sigma groups in our catalog, falls generally within the stated errors.

While we make choices to avoid fragmenting rich clusters with substructure, distinct but neighboring structures might also be artificially combined, resulting in more high-velocity dispersion (higher mass) groups in our catalog than expected. Thus, we examine the four clusters with $M_{vir} \geqslant 10^{15} M_\odot$ in our catalog to evaluate whether they are probably real or are the artificial combination of multiple groups and/or large-scale structure.

To do so, we verify if these groups are stable to changes in the velocity dispersion initial guess by comparing them in our catalog to that created using a initial velocity dispersion of 500 km s^{-1}. Of the four massive clusters, three are identical in both catalogs, and the other has group parameters that agree within the 3σ uncertainties. Additionally, three of these four have red sequences in their color–magnitude diagrams that suggest evolved clusters. The other might have a red sequence, but it is at low redshift and is thus poorly sampled. One of these also is a supergroup (see Section 5.2).

We also look at the 16 groups with the most bimodal member galaxy velocity distributions to determine whether each velocity peak corresponds to a distinct substructure on the sky. There is only one group that displays a well-defined distinction; we identify this group as a supergroup (see Section 5.2).

3.2. Comparison to Visual Identification

Early visual identification was used to construct a target group catalog for refining our group finding algorithm. Two of us (A.I.Z. and M.L.W.) studied the galaxy velocity histograms as well as the individual galaxy velocities and projected spatial positions in each field. We identified likely groups in 1500 km s^{-1} wide velocity bins in which at least 5 (A.I.Z.) or 10 (M.L.W.) galaxies were clustered on the sky relative to the surveyed field.

We used cases where our algorithm did not find visually identified groups to guide our parameter tuning and to understand the intrinsic limitations of the algorithm for this sample (e.g., the difficulty of identifying groups at higher redshifts). This check of course assumes that everything we identify visually is a real structure.

Our algorithm identifies visually identified groups in 69% of the peaks with at least 5 galaxies (91% of the peaks with at least 10 galaxies) and with strong clustering in both R.A. and decl. There are two possible general types of failures: the algorithm could be missing real structures that are well represented in our data (algorithm failure), or the algorithm could be missing structures because they are inadequately sampled (data failure). The visually identified groups that are not identified by the algorithm are typically located near the field edges, at higher redshift, or are located in regions of their field that are more densely sampled, which artificially causes the galaxies to appear clustered. Thus, data failure is the dominant cause for our algorithm to fail in identifying all our visually identified groups. Of all the velocity peaks in which our algorithm identifies structures, 11% were not visually identified. These groups do not have different properties than others found both visually and by our algorithm, except for those that have fewer members than we identified visually (the algorithmically identified groups with three and four members).

3.3. Additional Candidate Groups

Our magnitude-limited, multi-object spectroscopy is less successful at higher redshifts and in overdense cluster cores; this reduces the efficacy of our group-finding algorithm. To include additional structures for future spectroscopic follow-up or modeling in these fields, we create a supplemental candidate group catalog from our visual identifications. We focus on 58 single-redshift bins with $\geqslant 10$ galaxies clustered on the sky. For the additional candidate groups, we apply a simple 3σ clipping procedure (Yahil & Vidal 1977) to the galaxy redshift distribution within the bin to estimate group membership. We use no projected spatial criteria in this case. Once the 3σ clipping converges, we calculate the group virial radius. We then discard any members projected more than $3r_{vir}$ from the projected spatial centroid and recalculate all the group properties, including r_{vir}.

Four groups converge that include galaxies that have previously been assigned membership to algorithmically

selected groups (2 candidate group members in one case, 3 members in two cases, and all 13 members in one case). These galaxies are removed from the candidate groups, the group properties are recalculated, and the 3 that remain in the final catalog are flagged accordingly. Of the 58 redshift bins, 26 are rejected because their memberships did not converge or converged into groups with fewer than 3 members, they had fewer than 3 members within $3r_{vir}$, or they overlapped completely with a group in our algorithmic catalog.

We check the remaining groups with the most distinctly bimodal velocity distributions to determine whether they are separable on the sky; none have a velocity substructure that corresponds to distinct spatial substructure, therefore we do not remove any groups. Since the mean pairwise radial velocities at $r \sim 1$ Mpc for dark and luminous matter at $0 < z < 1$ are around $200 \, \mathrm{km \, s^{-1}}$ in the simulations of Weinberg et al. (2004), we discard an additional 9 candidate groups with $\sigma_{grp} < 200 \, \mathrm{km \, s^{-1}}$, as they could be merely cuts through filaments or sheets of galaxies rather than virialized groups.

We are left with 23 non-algorithmically selected candidate groups in our supplemental catalog. While we do not use color information to identify these structures, five have red-sequence-like galaxy overdensities in color–magnitude space. Thus, while incomplete sampling might make their identification and characterization more difficult, their assigned candidate group members very likely do trace evolved structures.

There are some redshift bins at higher redshift with fewer than 10 galaxies, but no identified groups. These are most likely parts of rich structures, since there are overdensities where our sensitivity is low. These peaks are in field b1422 at $z \sim 0.78$, in field b1600 at $z \sim 0.77$, in field he1104 at $z \sim 0.73$, and in field sbs1520 at $z \sim 0.72$ and 0.82. While we have enough galaxies in these redshift bins that there are noticeable peaks, we do not have enough to calculate meaningful candidate group quantities. We therefore make no further attempt to include them.

4. TESTING THE GROUP CATALOG

We perform tests to evaluate the quality of the group catalog produced by the group-finding algorithm.

4.1. Comparison of Individual Groups to the Literature

We compare our algorithmic catalog to group samples in the literature that overlap our fields. As the methods for identifying structures differ, this comparison tests the robustness of our catalog.

We compare our groups to groups and clusters in the NED within $20'$ of our field centers with spectroscopic redshifts that are not from previous work by our group. We consider a NED structure to be found if our group has a redshift within $3\sigma_z$ of the NED spectroscopic value. We do not compare other group properties, because ways of calculating them vary widely, they are not uniformly reported, and the survey footprints vary in size and position on the sky.

Three groups from NED that we do not recover are at redshifts that are either too high (2) or too low (1) to be readily detected given our redshift survey sensitivity, and four are in regions of their fields where we have little to no spectroscopic coverage. Of the remaining 26 entries, we find 17. For another 5, we find either substructures of the previously reported group,

or we combine known groups into one. We fail to find 4 groups. We explain this below.

Below we discuss those of our fields with groups listed in the NED.

b1600: Auger et al. (2007) find four groups in this field in their redshift sample of 40 galaxies. We find a group at $z \sim 0.29$ ($0.2893^{+0.0005}_{-0.0004}$ that agrees with their 0.291 group within their reported precision). We also find a group similar to their $z = 0.415$ group ($z_{grp} = 0.4146 \pm 0.0002$); five of our six group galaxies are added to our redshift sample from their work via the NED. We do not identify groups at $z = 0.540$ or 0.623, as they do; none of the galaxy redshifts from their $z = 0.291$, 0.540, or 0.623 groups are in Momcheva et al. (2015).

h12531: We find a group at $z_{grp} = 0.0531^{+0.0007}_{-0.0008}$, a similar redshift to Abell 3528 of the Shapley Supercluster (which has three entries in the NED at similar redshifts). Our group is very likely part of this larger cluster and has 13 of 22 member galaxies that have redshifts from the NED. Since the Abell cluster centroid is at the very edge of our field, we caution that the properties for our group might not be well determined.

hst14113: We recover a group at $z = 0.0808 \pm 0.0008$, near the $z = 0.0809$ group reported by Miller et al. (2005); 2 of our 26 members have redshifts added from the NED.

We also recover part of the 3C 295 cluster originally identified by Dressler & Gunn (1992) at $z = 0.4599$ with 112 galaxies and a velocity dispersion of $1300 \, \mathrm{km \, s^{-1}}$. We recover a group with 55 galaxies at slightly higher redshift (but still within the uncertainties: $z = 0.4603 \pm 0.0003$) and 2 small groups at slightly lower redshift (7 and 6 members at $z = 0.4504^{+0.0009}_{-0.0012}$ and $0.4592^{+0.0004}_{-0.0003}$, respectively). In our structures, only 9 galaxies (4 of 7 members of the $z = 0.4504$ group and 5 of 55 members of the $z = 0.4603$ group) are added from the NED.

lbq1333: We find a group at $z = 0.0856 \pm 0.0003$, near the $z = 0.085$ group reported by McConnachie et al. (2009); three of the five members have redshifts from the NED.

mg0751: the NED lists three groups with $z \sim 0.0266$. Although we are relatively insensitive to structures at such low redshift, we identify a group of four galaxies at $z = 0.0265^{+0.0002}_{-0.0001}$; one of these members has a redshift from the NED.

mg1549: We identify a group at $z = 0.0709$, as reported by Lopes et al. (2009); three of our seven members are from the NED.

pg1115: We find a structure at $z = 0.1600$, like that reported by Barkhouse et al. (2006) and Mason et al. (2000), including 6 (of 11) galaxies with redshifts from the NED.

We do not recover a group at $z = 0.477$ that has been attributed to WARPS-II by Mullis et al. (2003), but the more recent WARPS-II catalog of Horner et al. (2008) reports a redshift of 0.4859, where we do find a group; none of the 11 members have redshifts from the NED.

Carrasco et al. (2007) find a cluster at $z = 0.485$ made up of at least 2 substructures along the line of sight. We recover the substructure redshifts at $z = 0.48218$ and 0.49191 (our $z_{grp} = 0.4819^{+0.0007}_{-0.0006}$ and $0.4922^{+0.0007}_{-0.0005}$), but we do not find these 2 to be part of some larger cluster. All but 3 of the galaxies in these 2 of our groups (of 25 total members) are added from the NED.

rxj1131: Tucker et al. (2000) list 4 groups at $z = 0.0534$, 0.0966, 0.1014, and 0.1032. We find a group at $0.0531^{+0.0007}_{-0.0003}$, consistent with their lowest redshift group; none of our group members have redshifts from the NED. We also recover a group at $z = 0.1021 \pm 0.0004$, which is a combination of their other 3
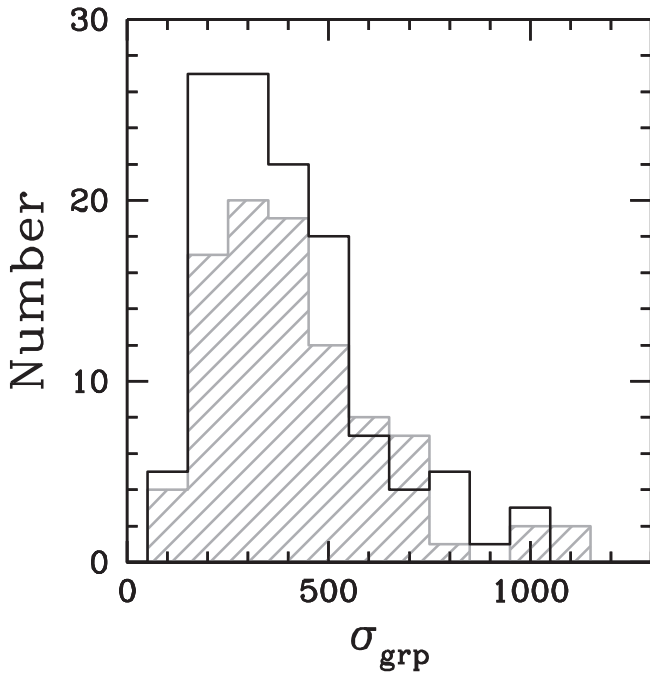
Figure 1. Comparison of the distribution of velocity dispersions between our group catalog (black histogram) and that of zCOSMOS (shaded gray histogram). For both catalogs, we select groups with $0.2 < z_{grp} < 0.5$ with at least five spectroscopically identified members and reported velocity dispersions. These distributions cannot be distinguished at the 95% confidence limit using a K-S test.

Figure 2. Comparison of our mass function for groups with $N_m \geqslant 5$ and $0.2 < z < 0.5$ (black points) with the Millennium Simulation mass functions (gray curves) at $z = 0.2$ (solid) and 0.5 (dotted). Bins are independent. Black error bars are the 1σ spread in the number of groups in a bin (not the error on the mean) using 1000 bootstrap realizations of our group masses and Poisson statistics. Gray error bars are the expected uncertainty in the observed counts that is due to cosmic variance given the simulation mass function at $z = 0.2$ using the Cosmic Variance Calculator (Trenti & Stiavelli 2008). The black points are normalized arbitrarily along the vertical axis so that the high-mass slope can be compared with the models (see text for details). The two highest mass bins do not have any observed groups, which is consistent with the model given the shot noise. The high-mass slope of our mass function agrees within the uncertainties with that of the simulation. Provided the normalization is reasonable, we therefore reliably find high-mass structures. Our catalog begins to suffer from incompleteness at masses lower than $\sim 10^{14}\ M_{\odot}$.

groups, but has a redshift within $3\sigma_z$ of their 2 higher redshift groups; 7 of the 66 galaxies in our group are from the NED.

sbs1520: Auger et al. (2008) find 3 groups ($z = 0.716$, 0.758, and 0.818). We only identify a group that is similar to the middle one; all 6 of our members are added from Auger et al. (2008). Our group at $z = 0.7590^{+0.0004}_{-0.0006}$ is much smaller than theirs (6 group galaxies to their 13). One complication is that we do not include the lens galaxy in our sample, because its redshift is ambiguous, while they do and assign it to this group. The most likely cause for the discrepancy, however, is their more permissive spatial selection. We are capable of recovering groups similar to their groups at $z = 0.716$ and 0.818 if we accept galaxies up to $5r_{vir}$ from the group centroid, which may not be bound to the group.

In summary, our group finder finds groups that are similar but not always identical to those in the literature in most cases.

4.2. Statistical Comparison of Group Properties to the Literature

While it is valuable to compare specific cases to ensure that our algorithm can recover previously reported structures, we also test whether the statistical properties of our group catalog are similar to those described elsewhere. Although we only discuss our algorithmic catalog here, including our non-algorithmic candidate groups does not significantly affect these comparisons.

4.2.1. Distribution of Group Velocity Dispersions

We compare our group catalog to that of zCOSMOS (Knobel et al. 2012) for groups with reported velocity dispersions and $0.2 < z_{grp} < 0.5$. We limit both samples to those with at least five spectroscopic members.

Using a Kolmogorov–Smirnov (K-S) test, we find that the resulting distributions of the velocity dispersions of the two catalogs are not distinguishable at the 95% confidence level (see Figure 1).

4.2.2. Frequency of Significant Substructure

For those of our groups with at least 10 members, we test for substructure using the Dressler–Shectman test (Dressler & Shectman 1988). This test calculates the difference between the average velocity of a galaxy and its nearest neighbors as projected on the sky compared with the mean velocity of the entire structure, as well as the difference between the local and global velocity dispersion. Spatial overdensities that correspond to velocity overdensities indicate substructure. We use 5000 Monte Carlo shuffles when calculating the probability that the Dressler–Shectman statistic Δ is observed by chance. Of our main group sample with $0.2 < z_{grp} < 0.5$, 55 groups have at least 10 members. Substructure is detected for 21 of these 55 groups (38%) at the $P < 0.05$ significance level.

Restricting our sample to only consider groups with at least 20 members (23 groups) and identifying $P < 0.01$ as significant, as do Hou et al. (2012), we find six have substructure (26%), in good agreement with the 27% (four of 15) found by Hou et al. (2012).

4.2.3. Distribution of Group Masses

We compare our group mass function to that of the Millennium-XXL (MXXL) Simulation (see Figure 2). MXXL is a high-resolution large-volume cosmological N-body simulation aimed at studying simulated cluster properties (Angulo et al. 2012). We calculate the mass function of our algorithmic catalog for the groups with $0.2 < z < 0.5$, $N_m \geqslant 5$, and $M_{\rm vir} \geqslant 10^{13}\, M_\odot$.

We wish to test (1) the shape of our mass function at high masses, where our group sample should be mostly complete, and (2) at which lower masses our sample is incomplete. Our mass function needs to be normalized by the volume probed by our sample to compare it to the simulations. However, because our redshift sample is not volume limited and there are large variations in spectroscopic completeness over each individual field and among fields, this normalization is not straightforward. Therefore, we searched for a normalization that allows the mass distribution shape to match the simulations in the highest mass bins and that represents a reasonable effective sample volume. We select a normalization using a χ^2 fit of the data at $M \gtrsim 10^{14}\, M_\odot$ assuming a two-sided Gaussian for the uncertainties in the data. The resulting fit has a $\chi^2 \sim 1$ and a $\sim 5'$ radius circular footprint per field. This footprint size corresponds to the $5'$ radius regions around the lenses that have the highest spectroscopic completenesses. Figure 2 shows this normalization of our data, which matches the simulations at high masses and also predicts a sensible field size. We conclude that the matched normalization is reasonable.

We calculate the simulation mass function using the Millennium Simulation cosmology and the fitting function of Angulo et al. (2012) using HMFcalc (Murray et al. 2013). We calculate their mass functions for $z = 0.2$ and $z = 0.5$ to bracket the redshift range for which we calculate our mass function. Our high-mass tail slope agrees with that of MXXL to within the uncertainties. Thus, we conclude that the number of high-mass objects we find is in agreement with theoretical expectations, provided the normalization of our mass function is reasonable, above roughly $10^{14}\, M_\odot$. Our mass function turns over at masses $\sim 10^{14}\, M_\odot$ and lower, indicating incompleteness in our group catalog at these masses.

4.2.4. Fraction of Galaxies in Groups

For our algorithmic group catalog, we calculate the fraction of all galaxies that are group members and compare it to the literature.

Carlberg et al. (2001) find over similar redshift (0.1–0.6) and velocity dispersion (40–700 km s^{-1}) ranges that 691 of 3290 (21% $\pm$ 1%, assuming Poisson errors) of their galaxies lie in groups of at least three members, where membership is defined within $1.5 r_{\rm vir}$ of the group centroid. To make a fair comparison, we consider our algorithmic groups with three or more members and similarly limit their membership to within $1.5 r_{\rm vir}$. We find that 1837 of our 9432 galaxies (19.5% $\pm$ 0.5%) are group members, consistent with Carlberg et al. (2001).

5. RESULTS

5.1. Group Catalog Properties

We present the group catalog in Tables 1 and 2, present group member galaxies in Appendix B (Table 5), plot the redshift and velocity dispersion distributions in Figure 3, and plot redshift histograms for each field in Figure Set 4. We also include sky plots and velocity histograms for each group in Appendix C (Figure Set 7).

In our algorithmic group catalog, we find 210 groups with at least 5 member galaxies, 186 of which are at $z \geqslant 0.1$. At redshifts below 0.1, our fields are not large enough to sample out to $r_{\rm vir}$ for any but the smallest groups. We therefore present groups at $z < 0.1$ with the caveat that the group properties, especially the group projected spatial centroid, might be poorly determined. Of the 210 at all redshifts, 187 have not previously been identified in the NED either by other authors or in work using earlier versions of our redshift catalog (Williams et al. 2006). We identify groups at $0.04 \leqslant z \leqslant 0.76$ with our range of greatest sensitivity at $0.2 < z < 0.5$ and a median at $z_{\rm grp} = 0.31$. Our groups have $60\,{\rm km\,s^{-1}} \leqslant \sigma_{\rm grp} \leqslant 1200\,{\rm km\,s^{-1}}$, with most (84%) with $100\,{\rm km\,s^{-1}} < \sigma_{\rm grp} < 600\,{\rm km\,s^{-1}}$. The median value is $\sigma_{\rm grp} = 350\,{\rm km\,s^{-1}}$.

From our experiments with our group algorithm (see Appendix A.1), we are not confident in the robustness of groups of three to four galaxies. Using geometric simulations of large-scale structure, Ramella et al. (1997) estimate that 50%–75% of their groups with three members are not gravitationally bound systems, while only 10%–30% of five or more member groups are spurious. As our algorithm only searches for groups in velocity bins and grid squares with at least five galaxies, three- and four-member groups are found only when there is another group at a similar redshift and position on the sky or when field galaxies are located nearby. However, we tabulate three- and four-member groups for completeness and for the information of future observational follow-up and gravitational lens modeling. We find 59 groups with three or four members at $0.03 \leqslant z \leqslant 0.76$ and a median redshift of 0.33. These groups have $20\,{\rm km\,s^{-1}} < \sigma_{\rm grp} < 270\,{\rm km\,s^{-1}}$ and a median of $140\,{\rm km\,s^{-1}}$.

We find one supergroup that we discuss in Section 5.2 and present in Table 3, Appendix B (Table 6), and Figure 5.

We present 23 additional candidate groups in Table 4, Appendix B (Table 7), and Appendix C (Figure Set 8) that were not identified by the algorithm. They span a range of $0.16 \leqslant z \leqslant 0.66$ with a median of 0.42, $220\,{\rm km\,s^{-1}} < \sigma_{\rm grp} < 1010\,{\rm km\,s^{-1}}$ with a median of $490\,{\rm km\,s^{-1}}$, and their median number of members is eight. The additional groups have on average somewhat higher velocity dispersions and mean redshifts than the $N_m \geqslant 5$ groups selected by our algorithm. Even at a given redshift, the non-algorithmic groups tend to have higher velocity dispersions. These differences arise from the sorts of groups we select with each method. We require at least 10 galaxies to be at a similar redshift to identify a possible non-algorithmic group where there is no algorithmic group. This choice selects for the richer groups missed by the algorithm. Non-algorithmic groups tend to have higher average redshifts, mainly because we only report those not found by our algorithm and the algorithm identifies most of the groups at low redshift.

We compare our group catalog to several group and cluster catalogs from the literature: CNOC2 (Carlberg et al. 2001), EDisCS (White et al. 2005), GAMA (Robotham et al. 2011), zCOSMOS (Knobel et al. 2012), and a flux-limited group catalog for SDSS galaxies (Tempel et al. 2014) (see Figure 6). While our catalog is similar to others in size, limiting magnitude, group velocity dispersions, and group redshifts, it is unique in that it is in fields of galaxy-scale strong gravitational lenses.
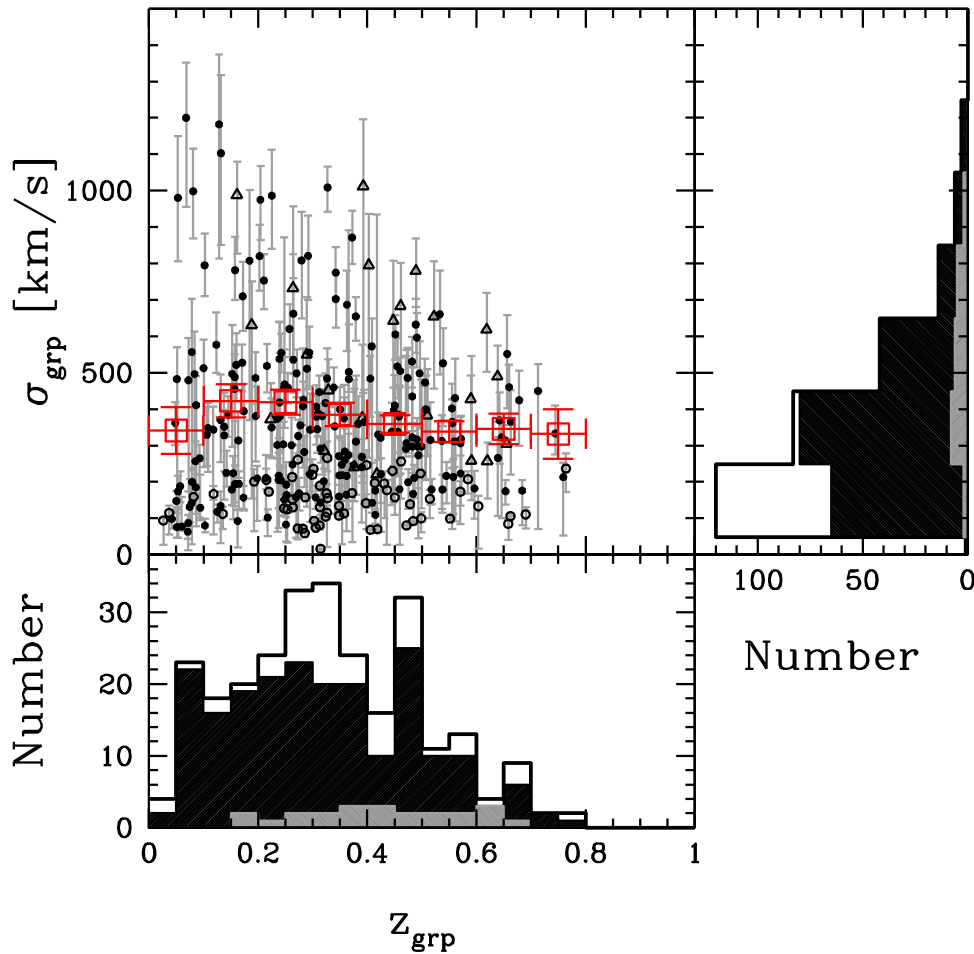
Figure 3. Velocity dispersion and redshift distributions for our group sample. Upper left: we show groups with at least five members (filled circles), those with three and four members (open circles), and the additional group candidates that are not found by our algorithm, but are visually identified (open triangles; see Sections 3.3 and 5.1). Open red squares denote the mean σ_{grp} derived from the filled circles; their red horizontal error bars show the 0.1 redshift bin width and vertical error bars the standard error in the mean. Lower left: redshift distributions for the 3+ member group sample (open histogram), the 5+ member group sample (solid black), and the additional group candidate sample (solid gray). The dip at $z_{grp} \sim 0.4$ corresponds to a decrease in the number of galaxy redshifts measured (see Figure 6 of Momcheva et al. 2015), which is most likely due to the Ca H and K absorption lines coinciding with the [O I] 5577 Å sky line. Upper right: velocity dispersion distributions for the same three samples. Our group catalog spans a range of velocity dispersions and redshifts, although most are in the $100 \text{ km s}^{-1} < \sigma_{grp} < 600 \text{ km s}^{-1}$ and $0.05 < z_{grp} < 0.55$ ranges. The dearth of higher redshift groups arises in part from the difficulty of spectroscopically sampling faint overdense group cores. The differences between the algorithmically selected and the supplemental visually identified samples are discussed in Sections 3.3 and 5.1.

5.2. Supergroup

In field b0712 our algorithm identifies a structure at $z_{grp} = 0.2941$ with the largest membership found in our sample (230 galaxies). However, it exhibits three clumps in projected spatial position and two distinct velocity peaks. While having clumps in space and velocity in clusters is reasonable if groups have fallen in, but have not completely virialized within the cluster, these clumps have projected spatial centroids that are several Mpc apart, on the order of or larger than the cluster virial radius. We therefore conclude that this structure is a supergroup, remove it from our final group catalog, and present its properties and those of its three main substructures in Tables 3 and 6 and in Figure 5.

Versions of this structure have been identified before. Fassnacht & Lubin (2002) find a much smaller group (ten members with $\sigma_{grp} = 306 \text{ km s}^{-1}$) at $z_{grp} = 0.2909$ with their smaller sample (~50 redshifts within several arcminutes of the lens). Momcheva (2009), using an earlier version of the redshift catalog we use, finds a large cluster (231 galaxies), but suggests it might either be a sheet of galaxies or several groups that are merging, similar to our interpretation.

In a different field, Smit et al. (2015) find a supergroup with similar properties to ours. Their super galaxy group at $z = 0.37$ has four component groups. The difference in group average velocity between the lowest and highest redshift components is about twice as large as the difference between ours, although when their outlying component is excluded, the velocity difference between the remaining lowest and highest redshift components is roughly five times smaller than ours. The projected spatial separations of their components are similar to our separation (a few Mpc). The component velocity dispersions are similar: ours range from 330 to 420 km s^{-1} and theirs from 303 to 580 km s^{-1}. However, our components have more identified members (39 to 54 galaxies compared to their 13 to 29). Our spectroscopic completeness over most of our field is comparable to theirs (as suggested by Gonzalez et al. 2005), although they have a much deeper limiting magnitude ($R \leqslant 22.5$), which means that our components are probably richer structures than theirs.

5.3. Lens Galaxy Environments

We find 12 of the 26 lens galaxies in our sample (46%) to be members of groups with at least 5 galaxies. These lenses are
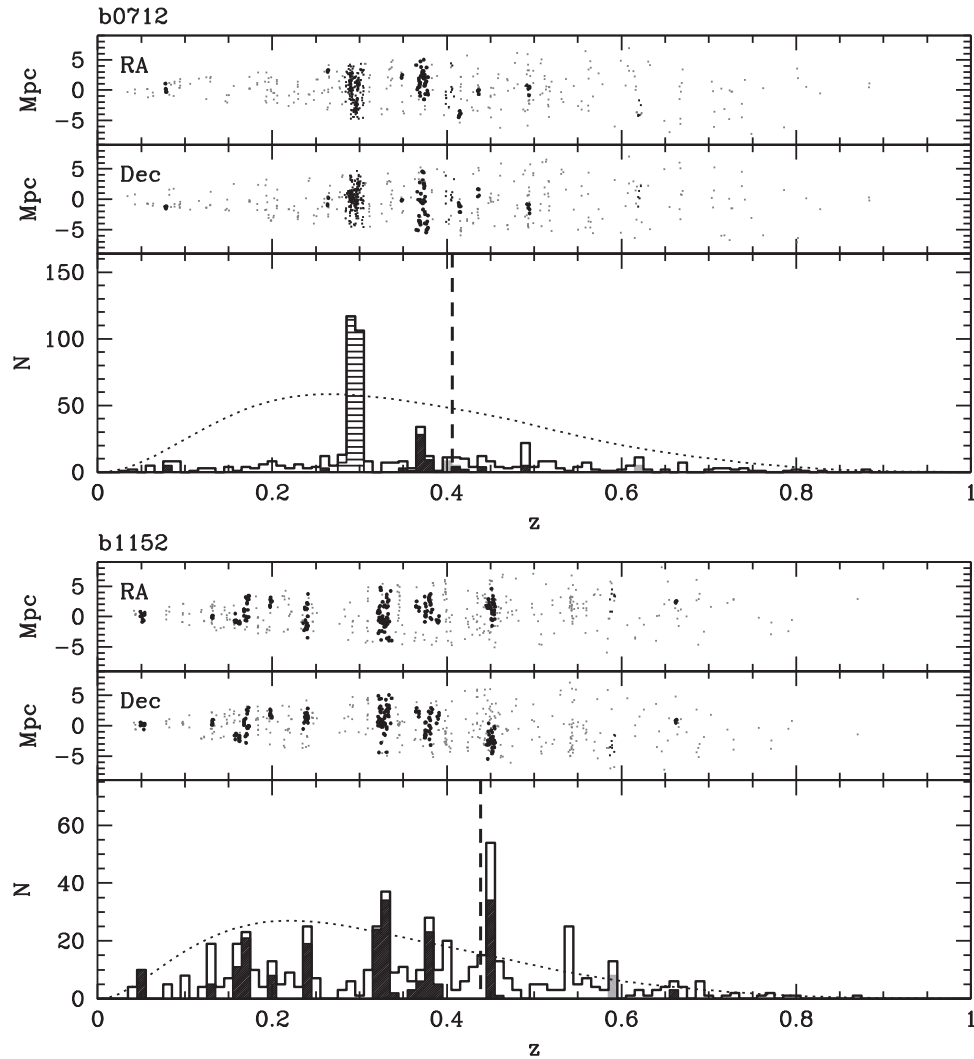
Figure 4. Redshift histograms for the 26 fields we include in our group catalog. The top two panels are the R.A. (top) and decl. (middle) offsets from the center of the field in Mpc at the redshift of the galaxy; the opening angles of the beams are exaggerated to show structure. The bottom panel shows the redshift distribution of the sample in redshift bins 0.01 wide, which corresponds to $\sim$2000 km s^{-1} at $z = 0.3$. The gray points and open histograms denote all the galaxies in our redshift catalog, the black circles and solid black histograms show the galaxies in our algorithmic group catalog (those listed in Tables 1 and 2), and the small black points and the solid gray histograms are our non-algorithmic candidate groups (Table 4). The large peak with the horizontally shaded histogram in field b0712 at $z \sim 0.29$ is the supergroup discussed in Section 5.2, Table 3, and Figure 5. The black dashed and dotted vertical lines indicate spectroscopic and photometric lens redshifts, respectively. The dotted curves are redshift selection functions arbitrarily normalized based on each field's most populated redshift bin. These functions are calculated using the spectroscopic field size and based on how the spectroscopic completeness varies over our I-band magnitude range for a homogeneous universe using the luminosity functions of Faber et al. (2007) for $0 < z < 1$, as in Ammons et al. (2014). These functions suggest where in redshift the spectroscopic samples for each field are most sensitive. Even when a group is not found at z_{lens}, there usually is more than one galaxy present.

(The complete figure set (26 images) is available.)

b1422, b1600, b2114, fbq0951, he0435, hst14113, mg0751, mg1654, pg1115, q0047, rxj1131, and wfi2033 (see Table 1 for group properties). One additional lens, b0712, is identified as a member of a non-algorithmic candidate group (see Table 4). While there are 2 non-algorithmic candidate groups near the lens redshift in field bri0952, the lens galaxy is not a member. Our percentage of lenses in groups with at least 5 galaxies agrees well with the 42% found by Momcheva (2009), who used redshifts drawn from an earlier version of Momcheva et al. (2015).

The remaining 13 lenses are not identified as group members but are most likely not isolated. Of these 9 lenses with firm spectroscopic redshifts, 5 have at least 5 other galaxies in the same redshift bin in Figure Set 4. Four (bri0952, he2149, mg1131, and q1355) are not in overdensities of galaxies, although 3 are at $z > 0.5$, where our redshift sample is much

less sensitive. Because of the ambiguity of the lens redshift in field sbs1520, we cannot conclude whether it is located in a group, but we do find galaxies near both possible redshifts. The remaining 3 lenses (h1413, h12531, and q1017) have only photometric redshifts, and they are not located in peaks of galaxies in the redshift number distribution.

5.4. Significant Line-of-sight Structures in Lens Fields

The importance of a line-of-sight structure to the lensing potential is affected by the structure mass and its proximity to the lens both in redshift and projected on the sky (Wong et al. 2011, 2012; McCully et al. 2016). We select groups and candidate groups within $2'$ of the lens, as Wong et al. (2011) found that most line-of-sight shear was caused by objects within this distance, and we select a high-mass threshold of

Table 3
Group Catalog Supplement: Supergroup and its Substructures in Field b0712

Group	N_m	z_{grp}	R.A. (deg)	Decl. (deg)	R^a (′)	σ_{grp} (km s^{-1})	M_{vir}^b ($10^{13}\,M_\odot$)	r_{vir} (Mpc)
0	230	$0.2941^{+0.0004}_{-0.0003}$	$108.9931^{+0.0152}_{-0.0137}$	$47.1480^{+0.0079}_{-0.0075}$	0.90	1170^{+40}_{-50}	$119.7^{+12.0}_{-13.6}$	2.48
1	54	$0.2898^{+0.0002}_{-0.0002}$	$109.1119^{+0.0144}_{-0.0133}$	$47.1527^{+0.0070}_{-0.0071}$	3.96	330^{+30}_{-30}	$3.7^{+1.1}_{-0.9}$	0.70
2	51	$0.2961^{+0.0002}_{-0.0002}$	$108.7460^{+0.0106}_{-0.0098}$	$47.1269^{+0.0070}_{-0.0078}$	11.06	340^{+30}_{-30}	$4.2^{+1.2}_{-1.0}$	0.73
3	39	$0.2983^{+0.0003}_{-0.0003}$	$109.0947^{+0.0111}_{-0.0110}$	$47.2807^{+0.0083}_{-0.0087}$	8.63	420^{+60}_{-60}	$7.1^{+3.0}_{-2.4}$	0.88

Notes.
[a] Projected distance between the lens and the group centroid.
[b] Mass assuming virialization.
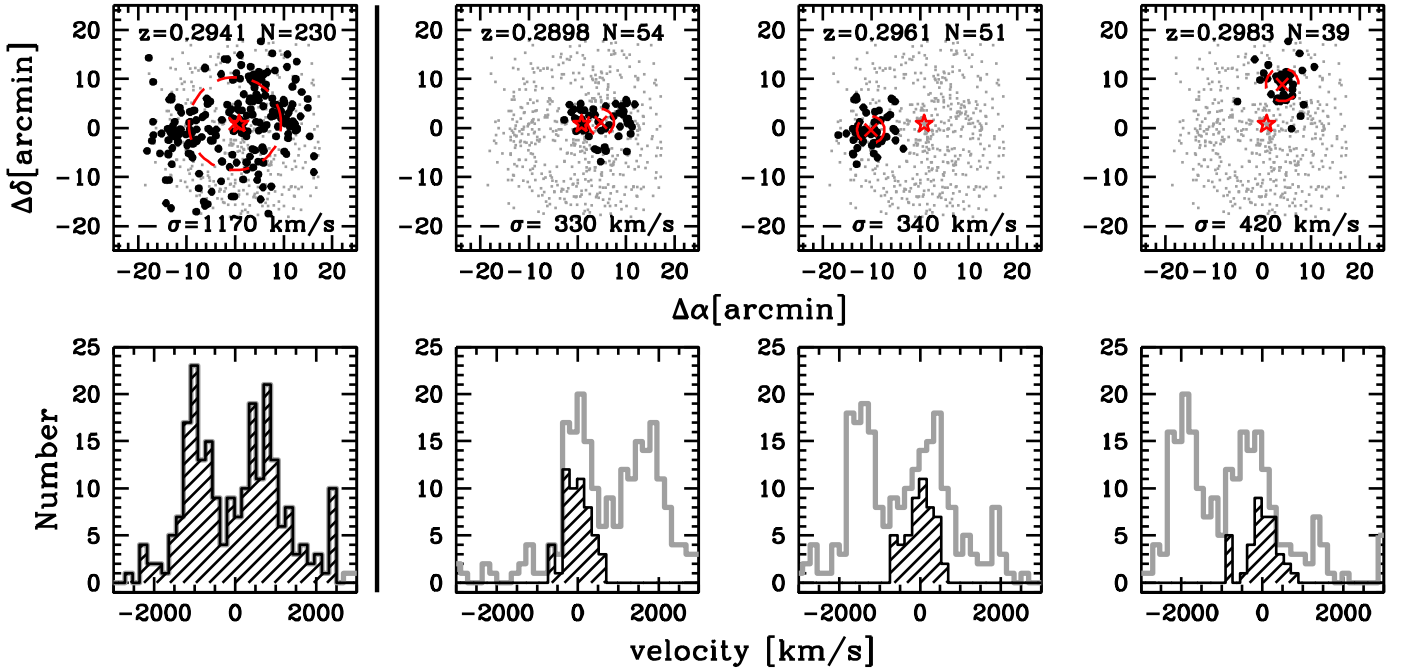
Figure 5. Top row: sky plots for the entire supergroup (leftmost column) and its three main substructures (other columns) in field b0712. Black points are group members, and gray points are the rest of the galaxies in the field in our redshift sample. Group redshifts, group velocity dispersions, and the number of group galaxies are marked. We also show the group projected spatial centroid (red cross), r_{vir} (red dotted circle), the lens (red star), and the angular size of 1 Mpc at the redshift of the group (black bar). Bottom row: Velocity histograms for these structures shifted so that the group mean velocity is at 0 km s^{-1}. Bin widths are 180 km s^{-1}, which corresponds to about three times the mean redshift error ($\sim$0.0002, or $\sim$60 km s^{-1}) at $z = 0.3$. Gray histograms are the full sample for the field, and black histograms are group galaxies. The group finder locates substructures that correspond to distinct regions both on the sky and in velocity.

$\sigma_{grp} \geqslant 500$ km s^{-1} to estimate how often line-of-sight structure might be important when determining the lensing potential. We do not include field b0712 because of the ambiguity that the supergroup provides; if this structure is one monolithic structure, it is very likely significant for the lensing, but if the three main substructures are better tracers of the mass, they are not as significant. For this analysis we therefore use a sample of 25 fields.

All but two of the systems for which a source redshift estimate is available have $z_{source} > 1$. This means that our group catalog is not sensitive to all mass between the observer and the source for most of these fields. French et al. (2014) find that their beams that most effectively lens $z \sim 10$ sources generally have significant halos with $0.1 < z < 0.6$ (single-halo beams) or $0.3 < z < 1.0$ (multi-halo beams). In addition, the mass between the main lens and the observer typically affects the lensing potential more than those between the main lens and the source (McCully et al. 2014). Since all our lens galaxies lie between $z = 0.1$ and 0.9, we are probably sensitive to the redshift range over which single groups might significantly affect the lensing potential as well as most of the redshift range for which multiple line-of-sight masses could be important.

In at least six of our 25 (24%) fields, there is at least one group or candidate group of which the lens is not a member that is likely to significantly affect the lensing potential. In future work, we will further quantify the importance of lens environments and and line-of-sight structures to the lensing models of these fields.

6. USING OUR GROUP CATALOG

While we make choices in our group-finding algorithm to balance completeness and contamination, we provide several tables and quality flags so that a user can tailor the group catalog for a particular science case. Here we give some
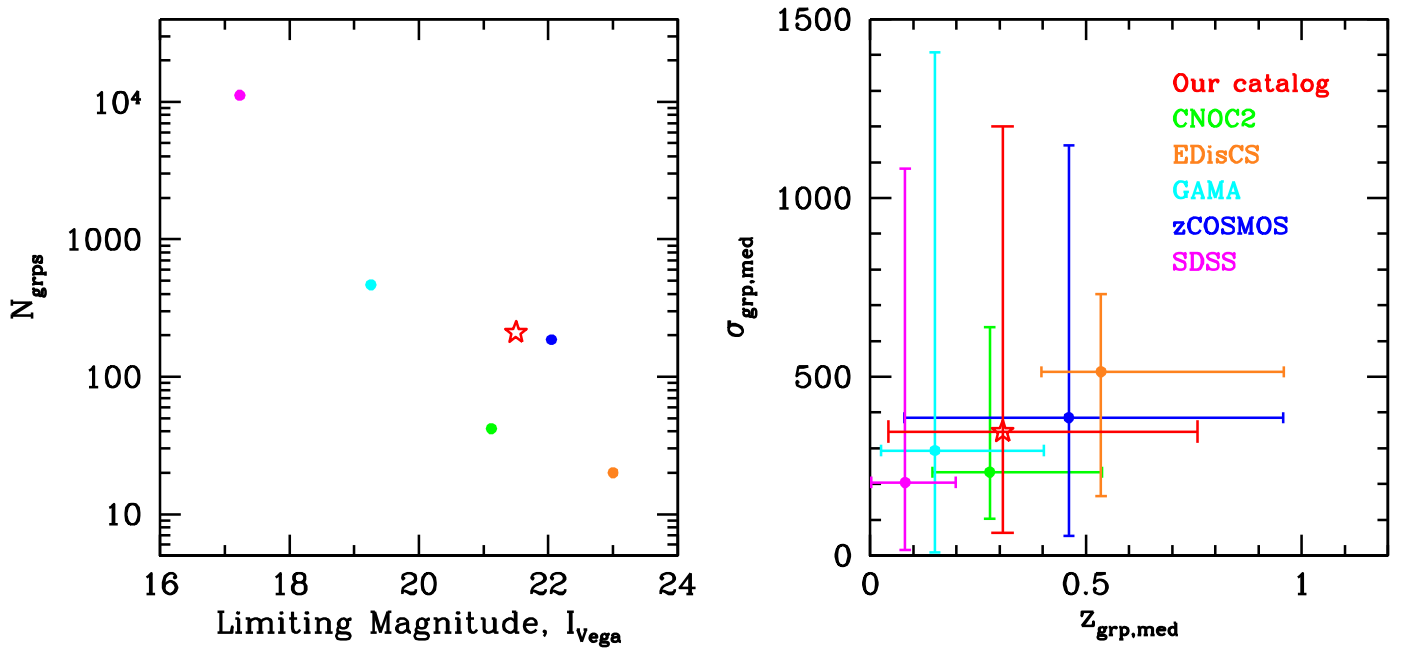
Figure 6. Comparison of our algorithmic group catalog (red stars) to others, including CNOC2 (green circles), EDisCS (orange), GAMA (cyan), zCOSMOS (blue), and an SDSS flux-limited catalog (magenta). Here we include only groups with $\geqslant$ five spectroscopic members and a reported velocity dispersion. Left: approximate limiting magnitudes for the redshift surveys used for each catalog transformed to I_{Vega} and the number of groups found. The red star represents our fainter limiting magnitude, which was used for the majority of the survey (Momcheva et al. 2015). Right: median velocity dispersions vs. redshifts for these group catalogs. Bars represent the total range in group properties. Our catalog has a number of groups for its limiting magnitude, redshift range, and velocity dispersion range comparable to the zCOSMOS group catalog. The uniqueness of our catalog is that it targets the fields of strong gravitational lensing galaxies.

suggestions of how to select subsamples of our catalog for various purposes.

Some of the groups in Table 1 have member galaxies quite close to the edge of their fields, and thus they might have group properties (primarily the projected spatial centroid) that are not well determined. Moreover, some are at redshifts such that they are not sampled out to at least r_{vir}. Therefore, to obtain the group sample with the highest confidence and the best-determined group properties, we suggest to use only groups in Table 1 with no flag (column 11). Such a subset would be well suited to studies of environmental effects on galaxy properties for which contamination is to be minimized. Additionally, when the poorest groups can be excluded in order to remove those most likely to be spurious, groups with $\sigma_{\mathrm{grp}} < 200\,\mathrm{km\,s^{-1}}$ could also be removed.

For lensing analyses of these fields, we suggest using all the information in Tables 1 and 4. We note that this choice will include groups at low redshift that we might not sample out to a virial radius or groups near the edge of our field with likely poorly determined spatial centroids.

To prioritize additional spectroscopic follow-up in these fields and thus to select galaxies that are likely to be at redshifts near our candidate groups, we recommend Tables 2 and 4. When the intention is to expand the footprint on the sky and thus interest is in groups that are detected on the edge of our observed fields or for which we do not sample out to at least r_{vir}, galaxies from Table 1 with flags of 1, 2, or 3 could also be included.

Users who wish to know of anything in these fields that could even possibly be a structure should use everything in Tables 1, 2, and 4 as well as either the first line (when the overall supergroup of b0712 is preferred) or the second through fourth lines (if the supergroup's main substructures are of interest) in Table 3. We note, however, that the resulting

composite will include groups that are identified in different ways.

7. CONCLUSIONS

We create a group catalog for 26 of the 28 gravitational lens fields in Momcheva et al. (2015). This catalog improves the characterization of the environments of the gravitational lenses and of line-of-sight groups and clusters in these fields, which will constrain how much such structures affect the lensing potentials.

We develop an iterative group finder for redshift samples with variable spectroscopic completeness levels and sampling footprints. We find 210 groups with at least 5 member galaxies in these fields. We newly identify 187 groups. These groups span $0.04 \leqslant z \leqslant 0.76$ with our range of greatest sensitivity at $0.2 < z < 0.5$ and a median of 0.31. Our groups have a velocity dispersion range of 60–1200 $\mathrm{km\,s^{-1}}$ with most between 100 and 600 $\mathrm{km\,s^{-1}}$ and a median of 350 $\mathrm{km\,s^{-1}}$. Our groups have from 5 to 66 members with a median of 8.

We test our group finder by comparing our group catalog to those in the same fields in the literature. We find groups similar to most ($\sim$85%) that were previously reported within our redshift range of sensitivity.

We also compare our groups' distribution of σ_{grp}, distribution of M_{vir}, incidence of substructure, and fraction of all sample galaxies that are group members to the literature. Our catalog agrees well with the empirical and theoretical expectations.

Our main results are as follows:

- We identify a supergroup in field b0712 with $z = 0.29$. This structure has three main components with 39 to 54 members and σ_{grp} from 330 to 420 $\mathrm{km\,s^{-1}}$ that occupy different regions projected on the sky and in radial velocity.

Table 4
Group Catalog Supplement: Visually Identified Candidate Groups

Field	Group[b]	N_m	z_{grp}[c]	R.A. (deg)	Decl. (deg)	R[d] (′)	σ_{grp} (km s^{-1})	M_{vir} ($10^{13} M_\odot$)	r_{vir} (Mpc)	Flag[e]
b0712	i[a]	13	$0.4030^{+0.0009}_{-0.0010}$	$108.9890^{+0.0362}_{-0.0306}$	$47.1460^{+0.0250}_{-0.0262}$	1.07	800^{+140}_{-530}	$39.5^{+18.6}_{-28.2}$	1.59	...
	ii	5	$0.6200^{+0.0005}_{-0.0005}$	$108.7936^{+0.0442}_{-0.0441}$	$47.1569^{+0.0223}_{-0.0223}$	9.06	260^{+50}_{-100}	$1.6^{+0.8}_{-0.9}$	0.46	...
b1152	i	8	$0.5897^{+0.0007}_{-0.0007}$	$178.9546^{+0.0350}_{-0.0391}$	$19.5294^{+0.0220}_{-0.0218}$	10.75	430^{+60}_{-180}	$6.4^{+2.7}_{-4.2}$	0.77	...
b2114	i	5	$0.3762^{+0.0004}_{-0.0005}$	$319.2515^{+0.0294}_{-0.0294}$	$2.4426^{+0.0338}_{-0.0363}$	2.51	240^{+220}_{-90}	$1.5^{+3.0}_{-0.1}$	0.49	...
	ii	6	$0.3911^{+0.0007}_{-0.0006}$	$319.3062^{+0.0354}_{-0.0289}$	$2.4526^{+0.0438}_{-0.0431}$	5.83	380^{+200}_{-160}	$5.0^{+6.7}_{-1.5}$	0.76	...
	iii	10	$0.4479^{+0.0009}_{-0.0008}$	$319.3432^{+0.0232}_{-0.0215}$	$2.4487^{+0.0451}_{-0.0437}$	7.97	640^{+160}_{-400}	$21.4^{+11.5}_{-8.8}$	1.25	...
bri0952	i	11	$0.6187^{+0.0009}_{-0.0010}$	$148.6635^{+0.0077}_{-0.0085}$	$-1.4307^{+0.0149}_{-0.0152}$	6.73	620^{+100}_{-120}	$17.5^{+8.1}_{-6.6}$	1.10	...
	ii	8	$0.6385^{+0.0009}_{-0.0008}$	$148.7207^{+0.0070}_{-0.0079}$	$-1.4832^{+0.0173}_{-0.0182}$	2.10	490^{+80}_{-120}	$9.1^{+4.5}_{-4.4}$	0.86	...
h12531	i	7	$0.5906^{+0.0006}_{-0.0005}$	$193.3469^{+0.0060}_{-0.0063}$	$-29.2643^{+0.0223}_{-0.0241}$	3.86	260^{+290}_{-110}	$1.6^{+5.1}_{-0.2}$	0.47	...
he0435	i	20	$0.2641^{+0.0005}_{-0.0006}$	$69.5769^{+0.0108}_{-0.0112}$	$-12.2579^{+0.0044}_{-0.0040}$	1.98	730^{+90}_{-240}	$33.8^{+11.6}_{-19.1}$	1.58	2
he1104	i	11	$0.4610^{+0.0008}_{-0.0009}$	$166.7501^{+0.0070}_{-0.0067}$	$-18.3619^{+0.0056}_{-0.0067}$	6.34	680^{+120}_{-460}	$25.2^{+11.8}_{-18.8}$	1.33	...
hst14113	i	28	$0.1616^{+0.0007}_{-0.0006}$	$212.6792^{+0.0278}_{-0.0237}$	$52.2742^{+0.0276}_{-0.0276}$	7.49	990^{+90}_{-160}	$81.0^{+19.3}_{-26.3}$	2.24	2
	ii	5	$0.3212^{+0.0004}_{-0.0004}$	$212.9999^{+0.0421}_{-0.0421}$	$52.1791^{+0.0254}_{-0.0255}$	6.22	290^{+60}_{-100}	$2.5^{+1.6}_{-1.5}$	0.60	...
	iii	9	$0.4175^{+0.0012}_{-0.0011}$	$212.8821^{+0.0526}_{-0.0446}$	$52.1198^{+0.0266}_{-0.0258}$	4.69	220^{+710}_{-110}	$1.2^{+51.0}_{-0.5}$	0.44	...
	iv	6	$0.5219^{+0.0012}_{-0.0012}$	$212.9382^{+0.0436}_{-0.0423}$	$52.3365^{+0.0269}_{-0.0296}$	9.53	650^{+150}_{-200}	$21.5^{+13.0}_{-9.6}$	1.23	...
mg1131	i	7	$0.2894^{+0.0008}_{-0.0008}$	$172.9468^{+0.0336}_{-0.0320}$	$4.8914^{+0.0501}_{-0.0503}$	3.28	550^{+160}_{-420}	$15.2^{+11.2}_{-8.6}$	1.17	...
q0047	i	3	0.6554	12.3979	−27.8512	1.96	310	2.5	0.53	4
q1017	i	11	$0.1884^{+0.0007}_{-0.0006}$	$154.3554^{+0.0213}_{-0.0229}$	$-20.8833^{+0.0093}_{-0.0092}$	6.03	630^{+120}_{-480}	$23.3^{+10.4}_{-13.6}$	1.41	3
	ii	10	$0.2234^{+0.0005}_{-0.0004}$	$154.3956^{+0.0155}_{-0.0168}$	$-20.8921^{+0.0089}_{-0.0089}$	7.04	370^{+100}_{-100}	$5.4^{+4.0}_{-2.5}$	0.82	3
rxj1131	i	17	$0.4890^{+0.0009}_{-0.0009}$	$172.9979^{+0.0260}_{-0.0273}$	$-12.5312^{+0.0233}_{-0.0242}$	1.96	780^{+90}_{-100}	$35.5^{+11.9}_{-10.5}$	1.49	4
wfi2033	i	6	$0.3288^{+0.0007}_{-0.0007}$	$308.5787^{+0.0179}_{-0.0159}$	$-47.3784^{+0.0071}_{-0.0071}$	6.34	450^{+90}_{-300}	$8.7^{+4.2}_{-5.7}$	0.94	...
	ii	13	$0.3926^{+0.0010}_{-0.0010}$	$308.5143^{+0.0358}_{-0.0373}$	$-47.3779^{+0.0235}_{-0.0242}$	3.79	1010^{+180}_{-570}	$76.9^{+30.6}_{-38.4}$	2.04	2, 4
	iii	6	$0.5100^{+0.0007}_{-0.0007}$	$308.4279^{+0.0172}_{-0.0178}$	$-47.4631^{+0.0075}_{-0.0069}$	4.08	380^{+130}_{-110}	$5.0^{+4.5}_{-2.0}$	0.72	3

Notes.
[a] A lens group.
[b] Numbering is not continued from Tables 1 and 2.
[c] Uncertainties are not calculated for $N_m < 4$
[d] Projected distance between the lens and the group centroid.
[e] (1) $z_{grp} < 0.1$ (groups at lower redshift are most likely not sampled out to r_{vir} because of the spectroscopic field size); (2) r_{vir} intersects the edge of the well-sampled region of the field because the group is large and/or at low z; (3) r_{vir} extends beyond the well-sampled region of the field because the group centroid or several of its members are located near the edge of the field; (4) group membership was adjusted manually to remedy overlapping membership.

- Of the 26 lenses in our sample for which we produce group catalogs, 12 (46%) are members of ⩾5 member groups (b1422, b1600, b2114, fbq0951, he0435, hst14113, mg0751, mg1654, pg1115, q0047, rxj1131, and wfi2033), and 1 (b0712) is identified as a member of an additional visually identified group candidate. These structures, which have σ_{grp} from 110 to 800 km s^{-1}, are likely to affect lensing models.
- In 6 of 25 (24%) of these fields that do not have the supergroup, there is at least one group or candidate group that does not include the lens galaxy with $\sigma_{grp} \geqslant 500$ km s^{-1} projected within 2′ of the lens, which likely affects the lensing potential.

Further analysis of the environments and line-of-sight structures of these lens fields will be discussed in a forthcoming paper.

APPENDIX A
CHOOSING PARAMETERS FOR OUR ALGORITHM

Here we describe the main parameters of our group-finding algorithm and how we choose them.

A.1. Candidate Peak Selection

There are several degenerate parameters that affect what types of groups can be identified as candidate peaks. The width of the bins in the galaxy velocity distribution affects how easily groups projected along the same line of sight can be distinguished. The grid square width in the galaxy sky position likewise affects how easily groups with similar radial velocities but different locations projected on the sky can be identified as

separate candidate peaks. If velocity bins or grid squares are too small, large and/or sparsely sampled structures (i.e., clusters and higher redshift structures) will be artificially fragmented and might not be identified as candidate peaks. If the bins or grid squares are too large, multiple structures might be identified as a single candidate peak. This conflation can also result in no group being identified if the average position and velocity of the galaxies are in sparsely populated regions. For both the velocity bins and sky grid, we need to decide how many galaxies must be in a bin or grid square to further consider that it might contain a group. If the threshold is set too high, we will only ever be able to find the richest structures. If it is set too low, we have a larger chance of including spurious groups in our sample.

Because we define the grid square sizes in terms of r_{vir}, where we use the relation for r_{200} given by Carlberg et al. (1997):

$$r_{vir,\sigma} \approx r_{200} = \frac{\sqrt{3}\,\sigma_{grp}}{10H(z)}, \qquad (5)$$

the initial velocity dispersion guess affects the properties above.

How the grid is centered is another choice. We place the center of a grid square at the median R.A. and decl. of the galaxies in each velocity bin to increase the likelihood that the best-populated structure in each velocity bin is centered in a grid square. However, the projected spatial distributions of galaxies in a given velocity bin are often complex, with multiple overdensities and/or a concentration plus a large diffuse component. Thus, we shift the grid to nine other positions (in units of a quarter of the width of a grid square in R.A., decl., and both) to increase the likelihood that multiple overdensities, where present, are centered in a grid square in at least one of the grid positions. Mismatches between galaxy overdensities and grid squares would primarily impact groups with few members in our redshift catalog and/or with members spread out on the sky; groups with up to eight members could be missed if they have their members split equally between two grid squares for all grid positions. If an overdensity is identified as a candidate peak but is not well centered in a grid square, then our subsequent iterative membership procedure can remedy this, as the projected spatial centroid is allowed to vary.

We test our method using velocity bins of 1000, 1200, 1500, 1600, and 2000 km s^{-1} and several grid square widths from $1.5r_{vir}$ to $5r_{vir}$. We set the galaxy number threshold at three and five galaxies for the velocity bins and three, four, and five galaxies for the spatial grid squares. We test using velocity dispersion initial guesses of 300, 400, and 500 km s^{-1}. Velocity bins of 1200 km s^{-1} width, grid squares of $3.3r_{vir}$ width, galaxy thresholds of five galaxies for both velocity bins and grid squares, an initial guess of the velocity dispersion of 400 km s^{-1}, and multiple grid positions are good parameters to distinguish multiple visually identified groups and avoid creating a large number of small most likely spurious groups or unphysically massive structures. While the majority of the catalog is robust for a grid square size within the range of 3–3.6 r_{vir} (tested in steps of 0.1 r_{vir}), we select the value that maximizes the number of recovered visually identified groups while minimizing the number of unphysically large structures.

Most of our groups have small velocity dispersions, with a peak in the number distribution at ~300 km s^{-1} (median value of 350 km s^{-1} for groups with at least five members) and a tail

Table 5
Algorithmic Group Members

Field	Group	z_{gxy}	ez_{gxy}	R.A.$_{gxy}$ (deg)	Decl.$_{gxy}$ (deg)
b0712	0	0.07849	0.00018	109.02408	46.84229
b0712	0	0.07773	0.00012	109.29465	46.89964
b0712	0	0.07797	0.00009	109.04527	46.85457
b0712	0	0.07865	0.00018	108.90497	46.89328
b0712	0	0.07866	0.00016	108.91337	46.91699

(This table is available in its entirety in machine-readable form.)

Table 6
Supergroup Members

Field	Group	z_{gxy}	ez_{gxy}	R.A.$_{gxy}$ (deg)	Decl.$_{gxy}$ (deg)
b0712	0	0.30306	0.00018	109.26192	47.09909
b0712	0	0.28987	0.00030	109.26274	47.11399
b0712	0	0.28954	0.00016	109.22754	47.18964
b0712	0	0.28460	0.00012	109.05324	47.01615
b0712	0	0.28980	0.00018	109.13190	47.06879

(This table is available in its entirety in machine-readable form.)

Table 7
Visually Identified Candidate Group Members

Field	Group	z_{gxy}	ez_{gxy}	R.A.$_{gxy}$ (deg)	Decl.$_{gxy}$ (deg)
b0712	i	0.40473	0.00023	109.32741	47.17129
b0712	i	0.40200	0.00030	108.78130	46.95694
b0712	i	0.40554	0.00030	108.99552	47.14788
b0712	i	0.40632	0.00018	109.29960	47.19134
b0712	i	0.40489	0.00023	108.96837	47.12892

(This table is available in its entirety in machine-readable form.)

to higher values (see Figure 3). To test how our assumption of 400 km s^{-1} for the initial velocity dispersion affects the final σ_{grp} distribution, we compare the results from our three velocity dispersion initial guesses. Overall, the catalogs are similar; the majority of groups have similar or identical calculated group properties. However, the 300 km s^{-1} catalog finds fewer groups, including 24 fewer visually identified groups. The 500 km s^{-1} catalog finds double the number of groups with $M_{vir} \geqslant 10^{15} M_{\odot}$, including one with an unphysical $M_{vir} = 5.6 \times 10^{15} M_{\odot}$ ($\sigma_{grp} = 1990$ km s^{-1}). The 400 km s^{-1} catalog agrees best with the velocity dispersion distribution from zCOSMOS, although none of these catalogs have distributions distinguishable from it using a K-S test. The 300 km s^{-1} catalog suffers from incompleteness when compared to the MXXL mass function at slightly higher masses than the 400 km s^{-1} catalog. The high mass slope of the 500 km s^{-1} catalog does not agree as well with that of MXXL due to its larger number of unphysically massive structures. Thus, we choose to use an initial velocity dispersion of 400 km s^{-1}.
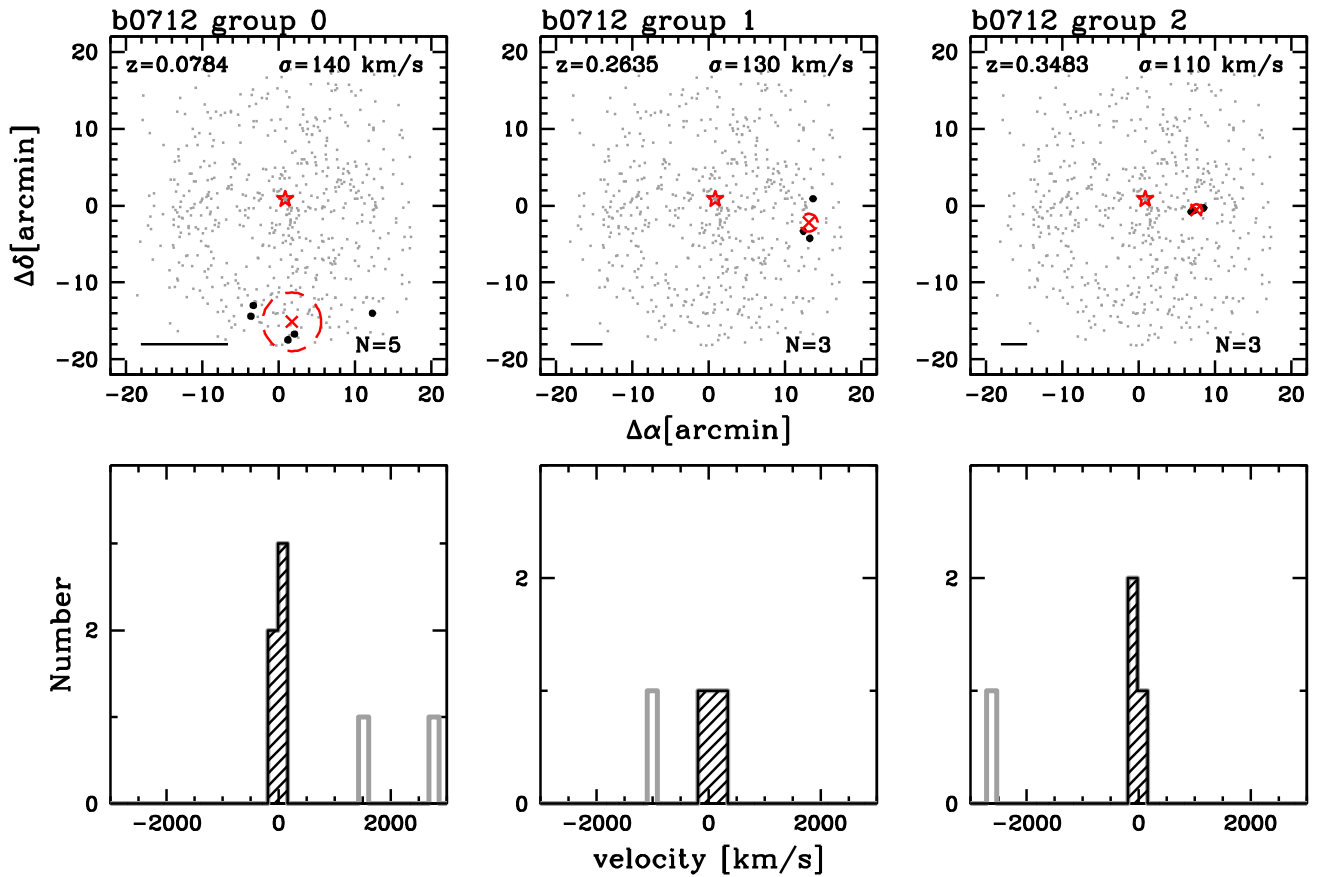
Figure 7. Top row: Sky plots for all groups in our algorithmic group catalog. Black points are group members, and gray points are the rest of the galaxies in the field in our redshift catalog (including galaxies in other groups). Group redshifts, group velocity dispersions, and the number of group galaxies are marked. We also show group projected spatial centroids (red cross), r_{vir} (red dashed circle), the lens (red star), and the angular size of 1 Mpc at the redshift of the group (black bar). Bottom row: Velocity histograms for our groups shifted so that the group mean velocity is at 0 km s^{-1}. Bin widths are 180 km s^{-1}, which corresponds to about three times the mean redshift error ($\sim$0.0002, or $\sim$60 km s^{-1}) at $z = 0.3$. Gray histograms are all galaxies in the redshift sample within $3r_{vir}$ of the group centroid, and black histograms are group galaxies. The dashed (dotted) vertical lines mark the velocities of the spectroscopic (photometric) redshifts of the lenses in the cases where the lens velocity is within 3000 km s^{-1} of the group velocity centroid, regardless of whether we identify the lens as a group member.

(The complete figure set (269 images) is available.)

A.2. Group Membership Iteration

We must select a redshift range Δz within which to look for possible group members. If Δz is too small, the velocity tails of massive structures get clipped, but if it is too large, large-scale structure might be misidentified as a group or cluster. We select Δz equivalent to 6600 km s^{-1} at the candidate peak redshift (using the special relativistic velocities) to include galaxies up to 3σ from the mean velocity for a cluster with a velocity dispersion of 1100 km s^{-1}, that of a Coma-like cluster. Very rare structures with even larger velocity dispersions can still be found by our algorithm, but their high-velocity tails will be somewhat clipped. Some small groups near larger structures in redshift also may be clipped. Even though most of our groups can be found using a smaller Δz, choosing 6600 km s^{-1} ensures that we properly sample the few massive clusters in our fields, so that their velocity dispersions and contributions to the lensing potentials are not underestimated.

In the first step of the group membership iteration, we must assume a velocity interval and a radius within which to consider possible group galaxies. We assume a velocity dispersion of 400 km s^{-1} and the virial radius relation given above for the same reasons given in the previous section.

For the final group catalog, we include galaxies projected up to $3r_{vir}$ from the group center on the sky. Including group members out to $3r_{vir}$ will likely increase the contamination by nonmembers, but it improves both our group and group member completeness. Both Carlberg et al. (2001) and Wilman et al. (2005) accept members out to $1.5r_{vir}$. The cosmological hydrodynamical simulations of Bahé et al. (2013) show that while beyond $3r_{vir}$ almost all galaxies are infalling into the host halos for the first time, some galaxies now at $\sim 3r_{vir}$ passed within $\sim 1r_{vir}$ earlier and thus have been influenced by the host halo.

We require the velocity dispersion to be at least 50 km s^{-1} for the structure to be considered a halo.

A.3. Duplicate Removal

We determine which groups include galaxies assigned to more than one group (overlapping members) in multiple trials. When at least 75% of the trials converge on an identical group, we add that group to our catalog. When a group is only found once among all the trials, it is discarded, because it is unlikely to be real. Any group that shares more than 50% of its membership with a group with at least twice as many members
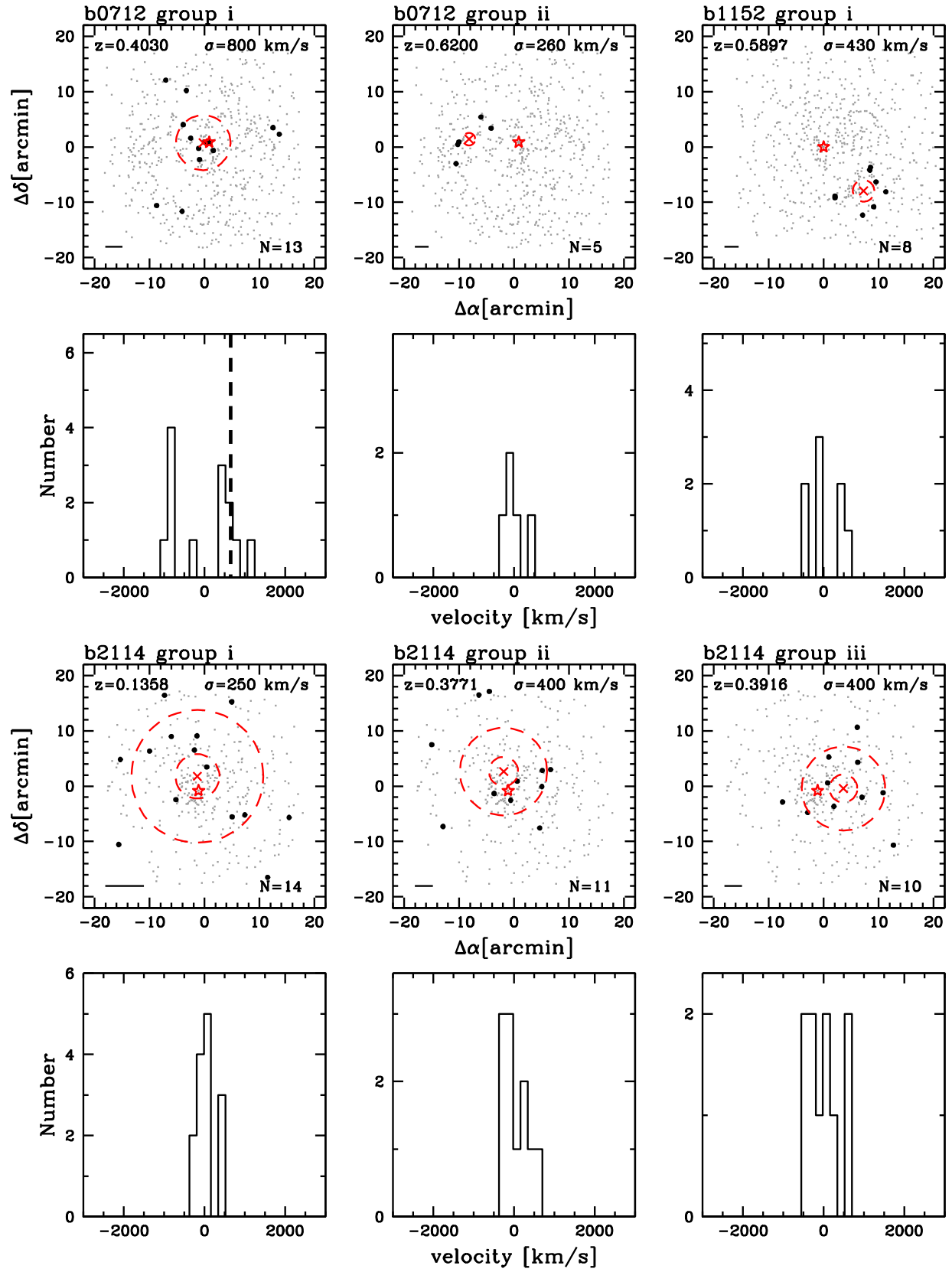
Figure 8. Same as Figure 7, but for the candidate groups. There are no gray histograms, since we use no spatial criteria for original candidate group identification. (The complete figure set (23 images) is available.)

is discarded, which prevents the artificial fragmentation of rich clusters. In other cases where a given group shares at least 50% of its members with another, we determine the mean group spatial centroid, the mean group redshift, the maximum group velocity dispersion, and the maximum group virial radius and reiterate on the group membership to produce the final group for the catalog.

The main parameters here are the percentage of group membership overlap and the fraction of groups found for a given candidate peak that must be identical to accept this group as is.

If the percentage of group membership overlap is set too high, then many galaxies are assigned to multiple groups. If it is set too low, we will combine groups that have most of their galaxies well separated, but have some outliers that overlap, which results in only one or neither group remaining in our catalog.

As most of the groups found among multiple trials either have identical membership or do not overlap at all, our catalog is fairly insensitive to our choice of group membership overlap fraction. Out of 53652 group membership overlap comparisons, only 238 (0.4%) have overlap fractions between 5% and 75%.

We rerun our membership iteration on those groups that have at least 50% overlapping membership with another group. Of these, 47 of 50 converge into 47 new groups. We remove the remaining 3.

After the second run of the membership iterator, there are seven pairs of groups that share a few member assignments (one galaxy in two cases, two galaxies in three cases, and three galaxies in two cases). To determine to which group these remaining galaxies belong, we calculate the offset in velocity and projected spatial position of each shared galaxy from its two possible groups using

$$R^2 = (v_{gxy} - v_{grp})^2 + (r_{gxy} - r_{grp})^2, \qquad (6)$$

where r_{gxy} is the position of the shared galaxy and r_{grp} is the group projected spatial centroid. The galaxy is assigned to the group for which R^2 is smaller, then the other group's properties are recalculated without that galaxy. We perform no further cuts on minimum velocity distribution or iterate further on membership. The groups with adjusted membership are flagged in Tables 1 and 2.

APPENDIX B
GROUP MEMBERS

Here we present the properties of group member galaxies (Tables 5, 6, and 7).

APPENDIX C
SKY MAPS AND VELOCITY DISTRIBUTIONS OF GROUPS AND CANDIDATE GROUPS

The sky maps and velocity distributions of our groups and candidate groups are available in Figure Sets 7 and 8.

REFERENCES

Ammons, S. M., Wong, K. C., Zabludoff, A. I., & Keeton, C. R. 2014, ApJ, 781, 2
Angulo, R. E., Springel, V., White, S. D. M., et al. 2012, MNRAS, 426, 2046
Auger, M. W., Fassnacht, C. D., Abrahamse, A. L., Lubin, L. M., & Squires, G. K. 2007, AJ, 134, 668
Auger, M. W., Fassnacht, C. D., Wong, K. C., et al. 2008, ApJ, 673, 778
Bahé, Y. M., McCarthy, I. G., Balogh, M. L., & Font, A. S. 2013, MNRAS, 430, 3017
Barkhouse, W. A., Green, P. J., Vikhlinin, A., et al. 2006, ApJ, 645, 955
Berlind, A. A., Frieman, J., Weinberg, D. H., et al. 2006, ApJS, 167, 1
Bertin, E., & Arnouts, S. 1996, A&AS, 117, 393
Biviano, A., Murante, G., Borgani, S., et al. 2006, A&A, 456, 23
Bleem, L. E., Stalder, B., de Haan, T., et al. 2015, ApJS, 216, 27
Carlberg, R. G., Yee, H. K. C., Ellingson, E., et al. 1997, ApJL, 485, L13
Carlberg, R. G., Yee, H. K. C., Morris, S. L., et al. 2001, ApJ, 552, 427
Carrasco, E. R., Cypriano, E. S., Neto, G. B. L., et al. 2007, ApJ, 664, 777
Chavushyan, V. H., Vlasyuk, V. V., Stepanian, J. A., & Erastova, L. K. 1997, A&A, 318, L67
Collett, T. E., Marshall, P. J., Auger, M. W., et al. 2013, MNRAS, 432, 679
Cool, R. J., Eisenstein, D. J., Fan, X., et al. 2008, ApJ, 682, 919
Demarco, R., Rosati, P., Lidman, C., et al. 2007, ApJ, 663, 164
Dressler, A., & Gunn, J. E. 1992, ApJS, 78, 1
Dressler, A., & Shectman, S. A. 1988, AJ, 95, 985
Faber, S. M., Willmer, C. N. A., Wolf, C., et al. 2007, ApJ, 665, 265
Fassnacht, C. D., & Lubin, L. M. 2002, AJ, 123, 627
French, K. D., Wong, K. C., Zabludoff, A. I., et al. 2014, ApJ, 785, 59
Gastaldello, F., Ettori, S., Molendi, S., et al. 2003, A&A, 411, 21
Girardi, M., Giuricin, G., Mardirossian, F., Mezzetti, M., & Boschin, W. 1998, ApJ, 505, 74
Gonzalez, A. H., Tran, K.-V. H., Conbere, M. N., & Zaritsky, D. 2005, ApJL, 624, L73
Gonzalez, A. H., Zaritsky, D., Dalcanton, J. J., & Nelson, A. 2001, ApJS, 137, 117
Haynes, M. P., Giovanelli, R., Martin, A. M., et al. 2011, AJ, 142, 170
Hinshaw, G., Weiland, J. L., Hill, R. S., et al. 2009, ApJS, 180, 225
Horner, D. J., Perlman, E. S., Ebeling, H., et al. 2008, ApJS, 176, 374
Hou, A., Parker, L. C., Wilman, D. J., et al. 2012, MNRAS, 421, 3594
Huchra, J. P., & Geller, M. J. 1982, ApJ, 257, 423
Jaroszynski, M., & Kostrzewa-Rutkowska, Z. 2012, MNRAS, 424, 325
Just, D. W., Zaritsky, D., Rudnick, G., et al. 2015, arXiv:1506.02051
Katgert, P., Mazure, A., Perea, J., et al. 1996, A&A, 310, 8
Keeton, C. R., Kochanek, C. S., & Seljak, U. 1997, ApJ, 482, 604
Keeton, C. R., & Zabludoff, A. I. 2004, ApJ, 612, 660
Knobel, C., Lilly, S. J., Iovino, A., et al. 2012, ApJ, 753, 121
Koester, B. P., McKay, T. A., Annis, J., et al. 2007, ApJ, 660, 221
Landolt, A. U. 1992, AJ, 104, 372
Lehar, J., Burke, B. F., Conner, S. R., et al. 1997, AJ, 114, 48
Limber, D. N., & Mathews, W. G. 1960, ApJ, 132, 286
Lloyd-Davies, E. J., Romer, A. K., Mehrtens, N., et al. 2011, MNRAS, 418, 14
Lopes, P. A. A., de Carvalho, R. R., Kohl-Moreira, J. L., & Jones, C. 2009, MNRAS, 392, 135
Marinoni, C., Davis, M., Newman, J. A., & Coil, A. L. 2002, ApJ, 580, 122
Mason, K. O., Carrera, F. J., Hasinger, G., et al. 2000, MNRAS, 311, 456
McConnachie, A. W., Patton, D. R., Ellison, S. L., & Simard, L. 2009, MNRAS, 395, 255
McCully, C., Keeton, C. R., Wong, K. C., & Zabludoff, A. I. 2014, MNRAS, 443, 3631
McCully, C., Keeton, C. R., Wong, K. C., & Zabludoff, A. I. 2016, arXiv:1601.05417
McGee, S. L., Balogh, M. L., Bower, R. G., Font, A. S., & McCarthy, I. G. 2009, MNRAS, 400, 937
Miller, C. J., Nichol, R. C., Reichart, D., et al. 2005, AJ, 130, 968
Momcheva, I., Williams, K., Keeton, C., & Zabludoff, A. 2006, ApJ, 641, 169
Momcheva, I. G., Williams, K. A., Cool, R. J., Keeton, C. R., & Zabludoff, A. I. 2015, ApJS, 219, 29
Momcheva, I. G. 2009, PhD thesis, The University of Arizona
Mullis, C. R., McNamara, B. R., Quintana, H., et al. 2003, ApJ, 594, 154
Munari, E., Biviano, A., Borgani, S., Murante, G., & Fabjan, D. 2013, MNRAS, 430, 2638
Murray, S. G., Power, C., & Robotham, A. S. G. 2013, A&C, 3, 23
Oguri, M. 2007, ApJ, 660, 1
Planck Collaboration, Ade, P. A. R., Aghanim, N., et al. 2016, A&A, 594, A27
Ramella, M., Pisani, A., & Geller, M. J. 1997, AJ, 113, 483
Refsdal, S. 1964, MNRAS, 128, 307
Robotham, A. S. G., Norberg, P., Driver, S. P., et al. 2011, MNRAS, 416, 2640
Smit, M., Schrabback, T., Velander, M., et al. 2015, A&A, 582, A82
Smith, A. G., Hopkins, A. M., Hunstead, R. W., & Pimbblet, K. A. 2012, MNRAS, 422, 25
Struble, M. F., & Rood, H. J. 1999, ApJS, 125, 35
Suyu, S. H., Auger, M. W., Hilbert, S., et al. 2013, ApJ, 766, 70
Szabo, T., Pierpaoli, E., Dong, F., Pipino, A., & Gunn, J. 2011, ApJ, 736, 21
Tanaka, M., Lidman, C., Bower, R. G., et al. 2009, A&A, 507, 671
Tempel, E., Tamm, A., Gramann, M., et al. 2014, A&A, 566, A1
Trenti, M., & Stiavelli, M. 2008, ApJ, 676, 767

Tucker, D. L., Oemler, A., Jr., Hashimoto, Y., et al. 2000, ApJS, 130, 237
Wambsganss, J., Bode, P., & Ostriker, J. P. 2005, ApJL, 635, L1
Weinberg, D. H., Davé, R., Katz, N., & Hernquist, L. 2004, ApJ, 601, 1
White, S. D. M., Clowe, D. I., Simard, L., et al. 2005, A&A, 444, 365
Williams, K. A., Momcheva, I., Keeton, C. R., Zabludoff, A. I., & Lehár, J. 2006, ApJ, 646, 85
Wilman, D. J., Balogh, M. L., Bower, R. G., et al. 2005, MNRAS, 358, 71

Wong, K. C., Ammons, S. M., Keeton, C. R., & Zabludoff, A. I. 2012, ApJ, 752, 104
Wong, K. C., Keeton, C. R., Williams, K. A., Momcheva, I. G., & Zabludoff, A. I. 2011, ApJ, 726, 84
Yahil, A., & Vidal, N. V. 1977, ApJ, 214, 347
Zabludoff, A. I., & Mulchaey, J. S. 1998, ApJ, 496, 39
Zabludoff, A. I., Zaritsky, D., Lin, H., et al. 1996, ApJ, 466, 104